Merlin controls the repair capacity of Schwann cells after injury by regulating Hippo/YAP activity.

Thomas Mindos[1], Xin-peng Dun[1], Katherine North[1,5], Robin D. S. Doddrell[1], Alexander Schulz[2], Philip Edwards[3], James Russell[1], Bethany Gray[1,5], Sheridan Roberts[1], Aditya Shivane[3], Georgina Mortimer[1] , Melissa Pirie[1], Nailing Zhang[4], Duojia Pan[4], Helen Morrison[2] and David B. Parkinson[1].

1. Plymouth University Peninsula Schools of Medicine and Dentistry, Derriford, Plymouth, Devon, UK, PL6 8BU.

2. Leibniz Institute for Age Research-FLI Jena, Beutenbergstr. 11, D-07745, Jena, Germany.

3. Department of Cellular and Anatomical Pathology, Derriford Hospital, Plymouth, UK.

4. Howard Hughes Medical Institute, Department of Molecular Biology and Genetics, Johns Hopkins University School of Medicine, United States.

5. University of Bath, Claverton Down, Bath, UK, BA2 7AY.

Correspondence to: Prof. David Parkinson, Plymouth University Schools of Medicine and Dentistry, Derriford, Plymouth, Devon, UK PL6 8BU.

Tel. 0044 (0)1752 431037; Fax 0044 (0)1752 517846

e-mail: david.parkinson@plymouth.ac.uk

Condensed title: Schwann cell Merlin controls repair of the PNS.

eTOC: The regenerative capacity of Schwann cells in the PNS underlies functional repair following injury. Here, Mindos et al show a new function for the tumour suppressor Merlin and Hippo/YAP signalling in the generation of repair-competent Schwann cells following injury.

Number of characters: 39,838

Abstract.

Loss of the Merlin tumour suppressor and activation of the Hippo signalling pathway play major roles in the control of cell proliferation and tumourigenesis. We have identified completely novel roles for Merlin and the Hippo pathway effector Yes Associated Protein or YAP in the control of Schwann cell plasticity and peripheral nerve repair following injury. Injury to the peripheral nervous system (PNS) causes a dramatic shift in Schwann cell molecular phenotype and the generation of repair-competent Schwann cells, which direct functional repair. We find that loss of Merlin in these cells causes a catastrophic failure of axonal regeneration and remyelination in the PNS. This effect is mediated by activation of YAP expression in Merlin null Schwann cells and loss of YAP restores axonal regrowth and functional repair. This work identifies new mechanisms that control the regenerative potential of Schwann cells and give a new insight to understanding the correct control of functional nerve repair in the peripheral nervous system.

Introduction.

While the peripheral nervous system (PNS) may repair effectively following injury, such repair relies upon both the neurons and Schwann cells (SCs) to hugely change their roles from a function that supports normal nerve transmission to a function supporting repair and regeneration (Jessen and Mirsky, 2016; Jessen et al., 2015; Kim et al., 2013). The generation of repair-competent SCs distal to the site of the injury, termed Büngner cells, involves the transcription factor cJun-dependent loss of myelin proteins, recruitment of macrophages and the activation of the specific repair programme in SCs (Arthur-Farraj et al., 2012; Jessen and Mirsky, 2016; Parkinson et al., 2008). The slowed axonal regeneration that occurs in older mice is also associated with an impaired induction of cJun and reduced myelin clearance in SCs following injury (Kang and Lichtman, 2013; Painter et al., 2014). Injury to the PNS also triggers the activation of mitogen activated protein kinase (MAPK) pathways within SCs, such as the extracellular regulated kinases (ERK) 1/2 and p38 pathways and signalling through these pathways regulates the de-differentiation of SCs and immune cell entry into the nerve following injury (Harrisingh et al., 2004; Napoli et al., 2012; Yang et al., 2012).

The Merlin tumour suppressor has been well characterised for its roles in controlling cell signalling, contact mediated inhibition of growth and tumourigenesis. Loss of function of Merlin, either sporadically or in the inherited condition of Neurofibromatosis type 2 leads to the formation of tumours within the nervous system, including schwannomas, meningiomas and ependymomas in affected individuals (Hanemann, 2008; Hilton and Hanemann, 2014). Loss of Merlin leads to dysregulation of many cell processes including control of the $CRL4^{DCAF1}$ E3 ubiquitin ligase, regulation of MAPK signalling and a decrease in Hippo signalling pathway

leading to increased activity of the Hippo effectors Yes Associated Protein (YAP) and Transcription co-activator with PDZ-binding motif (TAZ) (Ammoun et al., 2008; Cooper and Giancotti, 2014).

While much of the research has focussed upon the role of Merlin in schwannoma formation, many patients with NF2 also have a peripheral neuropathy and it has been shown that expression of the Merlin isoform 2 within the neurons of the PNS is necessary for maintaining axonal integrity through maintaining correct neurofilament heavy chain phosphorylation (Schulz et al., 2013). More recently, axonal Merlin has been also been shown to regulate neuregulin 1 type III expression on PNS axons and expression of the ErbB2 receptor on SC (Schulz et al., 2014a). The combined axonal and SC heterozygosity for Merlin in patients with neurofibromatosis type 2 has also been proposed as a likely contributor to potential tumour formation in the peripheral nervous system (Schulz et al., 2016).

Although the generation of Merlin null SC tumours, schwannomas, in the peripheral nervous system (PNS) has been well studied, the function of Merlin-dependent signalling in the processes and control of PNS regeneration and repair has not been fully investigated. Using a sciatic nerve crush model of nerve repair in mice with SC-specific deletion of Merlin, we find that Merlin function is crucial for the generation of the repair-competent SCs, which facilitate axonal regeneration and functional repair in the PNS. We observe significant increases in SC proliferation and macrophage infiltration in Merlin null nerves, a severely impaired axonal regeneration and remyelination, together with a reduced induction of cJun following injury. In addition to this, analysis of signalling in Merlin null nerves following injury shows changes in MAP kinase signalling and a specific injury-dependent activation of YAP in Merlin null SCs. We have further tested the significance of this altered Hippo pathway

signalling and show, remarkably, that removal of YAP alone functionally corrects the PNS repair defects seen in Merlin null nerves, restoring cJun and neurotrophin expression together with axonal regeneration and functional recovery following injury. These findings identify completely novel functions for both Merlin and the YAP protein in the regenerative capacity of the PNS and may point to potential new ways to boost PNS function and repair in disease or following injury.

Results.

Loss of Merlin in Schwann cells causes a transient hypomyelination in the peripheral nervous system.

Little is known about the effects of Merlin loss upon the control of SC development and myelination, although previous studies in Merlin conditional null animals have assessed the potential for schwannoma tumour development. (Denisenko et al., 2008; Gehlhausen et al., 2015; Giovannini et al., 2000). Using the well characterised mP_0TOTA-CRE (P0-CRE) line to specifically remove Merlin in SCs of the PNS at E13.5 (Feltri et al., 1999), we first tested the roles of Merlin in controlling SC myelination and cell number. Analysis of myelination at post-natal day (P) 6 showed a hypomyelination of the sciatic nerve in mice with SC-specific loss of Merlin by both electron microscopy (EM) and western blot analysis (Figs. 1 A, B and E and S1 D). Numbers of SCs were slightly but significantly raised in Merlin null animals at both P6 and in adult animals (Figs. 1 F and S1 E-G) and in confirmation of previous data (Denisenko et al., 2008), we also observed a shorter internodal distance together with increased numbers of Schmidt-Lanterman incisures in the peripheral nerves of Merlin null animals at P60 (Fig. S5 H-M). Analysis of P21 and P60 nerves showed that by these later timepoints, however, myelination appeared normal with only small non-significant differences in myelin thickness (G ratio) between control and Merlin null animals and comparable myelin protein expression (Figs. 1 C, D, G, S1 A-C, 2 M and 9 F). All measures of peripheral nerve function such as nerve conduction velocity, compound muscle action potential and functional testing of animals using a rotarod to check sensory-motor co-ordination showed no significant differences between adult control and Merlin null animals (Figs. 5, E-G and S5 G).

Loss of Merlin in Schwann cells causes a failure of regeneration and remyelination following injury.

Injury to the peripheral nervous system starts a series of well characterised events distal to the site of the injury that include degeneration of axons, immune cell infiltration and reprogramming of SCs to assume a repair-competent state (Arthur-Farraj et al., 2012; Jessen and Mirsky, 2016; Kim et al., 2013). As Merlin is a key regulator of cell signalling, we analysed the control of repair following crush injury in sciatic nerve with SC-specific deletion of Merlin.

For Merlin null nerves we observed a large decrease in the numbers of regenerating axons and almost no remyelination as compared to controls (Fig. 2 C-L); we also observed a significant expansion of the entire nerve distal to the site of injury (Fig. 2 A, B and G-J). Corresponding to the lack of remyelination, western blotting for myelin basic protein (MBP) showed almost undetectable levels in Merlin null distal nerves at 21days (d) following injury, but MBP was re-expressed in control nerves demonstrating the onset of remyelination in these animals (Fig. 2 M). Even at 60d post-crush injury, axonal regeneration and remyelination were both very poor in Merlin null nerves as compared to controls (Fig. 2 I, J and L).

Numbers of regenerated axons within the tibial nerve showed a large reduction in Merlin null animals at both 21d and 60d following injury and those axons that do regenerate associated poorly with SCs (Fig. 3 A-F). Even when larger diameter axons regenerate into the distal tibial Merlin null nerve, they were poorly myelinated with increased G ratios at both 21d and 60d after crush injury (Fig. 3 G, H). Following injury we also observed greatly increased numbers of SCs, which displayed extensive cellular processes; many SCs ensheathed groups of collagen fibres (Fig. 3

B, D, I and J). Even when correctly associating with and myelinating an axon, Merlin null SCs exhibited the same multiple cell processes and discontinuous basal lamina (Fig. 3 I). To test whether this SC behaviour within the Merlin null distal nerve may be due to the lack of regenerating axons, we performed experiments in which a section of nerve was removed to prevent axonal regeneration into the distal stump. We never observed such SC behaviour or collagen wrapping in control animals, even at 60d post injury (unpublished data), indicating that this effect was specific to nerves containing Merlin null SCs and not an effect of the continued absence of axons within the nerve distal to the crush site.

We next extended this analysis to an even longer timepoint of 8 months post-crush injury. Remarkably, even at this time, analysis of distal nerve samples from Merlin null animals still showed a lack of axonal regeneration and re-myelination, demonstrating that the regeneration defect does not correct in nerves containing Merlin null SCs (Fig. S2 A-H). Staining with Masson's trichrome stain also revealed the large amount of collagen within the injured Merlin null nerves at this timepoint. (Fig. S2 I-J). Together, these findings show a crucial role for the Merlin in SCs to generate the repair-competent Büngner cells required for efficient axonal regeneration and remyelination following injury to the PNS.

<u>Reduced axonal regeneration, elevated cell proliferation together with increased and sustained macrophage numbers in Merlin null nerves following injury.</u>

We have previously described the use of wholemount staining to visualise axonal regeneration following both cut and crush injuries (Dun and Parkinson, 2015). Using this technique, we saw that the distance of the leading regenerating axon was significantly reduced in Merlin null nerves at 7d post-crush injury (Fig. 4 A-C). Using

neurofilament staining to identify regenerating axons in transverse sections of sciatic nerve distal to the injury site, there was a clear reduction in the numbers of regenerating axons in the distal sciatic nerve at both 7d and 21d post-crush injury in Merlin null nerves (Fig. 4 D-G).

Injury to peripheral nerves induces distal SC demyelination and proliferation, breakdown of the blood-nerve barrier and consequent macrophage influx to the nerve (Jessen and Mirsky, 2016). We found that post-crush injury at 7d, both proliferation, measured by Ki67 labelling, (Fig. 4 H) and macrophage numbers, measured by Iba1/F4/80 double labelling (Iba1 staining shown), were significantly elevated in Merlin null nerves. Even at later timepoints, 21d and 60d post-injury, significantly more macrophages were present within Merlin null nerves (Fig. 4 I-K), demonstrating an ongoing inflammatory response in these animals.

Loss of functional recovery in Merlin null nerves.

Next, we used a number of measurements to assess functional recovery in Merlin null nerves following injury. Following a sciatic nerve crush injury, control animals recover function fully by 21d as previously reported (Arthur-Farraj et al., 2012; Yang et al., 2008) (Fig. 5 A) and our analysis of the tibial nerves from control animals show normal axonal regeneration and remyelination at this timepoint (Fig. 2 G). Assessment of functional recovery by the static sciatic index (SSI), a gait analysis which measures sensory-motor recovery (Baptista et al., 2007), showed no functional recovery at 21d in Merlin null animals as compared to a full recovery by control animals using this test (Fig. 5 A). Analysis of functional recovery using single frame motion analysis of both foot-base angle and lateral foot-base angle, to measure recovery of motor function (Fey et al., 2010), both showed significant

deficits in function in Merlin null animals at 35d and foot-base angle at 105d post-injury, confirming the long-term loss of nerve function in these animals (Fig. 5 B-D). Furthermore, measurements of both nerve conduction velocity and compound muscle action potential, to assess axon regeneration, re-innervation and remyelination, in nerves 35d after crush injury showed significant reductions in Merlin null animals (Fig. 5 E-G). Measures of the recovery of sensory function in the foot by the toe pinch test also showed little or no recovery even at 35d in Merlin null animals as compared to control animals that showed full recovery at 21d (Fig. S3).

Alterations in Hippo pathway signalling, cJun expression and MAP Kinase activation in Merlin null nerves following injury.

The poor axonal regeneration seen in Merlin null animals partly resembles that seen in animals with SC-specific loss of the transcription factor cJun, although there are also clear differences in the phenotypes between these two transgenic lines, for instance the increased macrophage infiltration seen in Merlin null nerves is not seen in cJun null nerves following injury (Arthur-Farraj et al., 2012).

Measurement of cJun protein levels in Merlin null nerves showed a reduced induction of cJun protein at 4d, 7d and 11d post-crush injury (Fig. 6 A, B and D) and at 7d post-transection injury (Fig. 6 C) in Merlin null animals by both immunolabelling and western blotting. In the nerve crush experiments, as cJun levels began to drop at 21d post-crush injury in control animals, presumably reflecting the remyelination of the distal nerve, weak cJun expression was maintained in Merlin null animals at this timepoint, underlining the lack of re-myelination seen (Figs. 2 H, M and 9 F). In keeping with this effect and lack of remyelination in Merlin null animals, we observed increased levels of the immature SC marker N-cadherin in Merlin null animals at later

timepoints following injury and reduced levels of E-cadherin (Fig. 6 D); E-cadherin is induced in SCs as they begin to myelinate (Crawford et al., 2008). In addition we saw increased levels of active beta-catenin in Merlin null nerves following injury.

Although we observed reduced levels of cJun in Merlin null SCs following injury, we did not observe *in vitro* nor *in vivo* the delayed dedifferentiation and loss of myelin proteins seen in cJun null animals at 7d post-transection injury (Fig. 6 C and unpublished data).

Induction of the SC chemokine monocyte chemoattractant protein 1, MCP1/CCL2, is known to be important for entry of macrophages into the nerve following injury and is regulated by activity of the MEK/ERK1/2 pathway in SCs; in addition, activation of the p38 MAP kinase pathway has been implicated in macrophage recruitment and activation following injury (Fischer et al., 2008a; Myers et al., 2003; Napoli et al., 2012; Tofaris et al., 2002). Activity of both the ERK1/2 and p38 MAP kinase pathways were elevated in Merlin null nerves following both crush and transection injury, as well as levels of MCP-1 protein (Fig. 6 C, D), in accordance with the increased numbers and persistent presence of macrophages within the Merlin null nerves following injury (Fig. 4 I-K).

<u>The failure of Merlin null nerves to repair is dependent upon activation of the Hippo pathway effector YAP.</u>

A key function of the Merlin tumour suppressor in cells is to regulate activity of the Hippo pathway. The Hippo pathway effectors YAP and TAZ are phosphorylated by the LATS1/2 kinases which inactivates their function by increasing YAP/TAZ retention in the cytoplasm (Cooper and Giancotti, 2014). Loss of Merlin in tumour cells leads to increased YAP/TAZ-dependent signalling and the formation of Merlin

null liver tumours requires YAP function (Zhang et al., 2010). Western blotting of distal nerve samples post-injury showed an increase in YAP levels only in Merlin null nerves following injury, whereas for TAZ we saw an increase in levels in both control and Merlin null animals, albeit at higher levels in the Merlin null animals (Fig. 6 D). The level of connective tissue growth factor, CTGF, which is a Hippo target (Shimomura et al., 2014; Zhao et al., 2010), was also strongly increased, together with raised levels of collagen type IV in Merlin null nerves after injury (Fig. 6 D).

Given the strong injury-specific activation of YAP in Merlin null nerves, we next tested the effects of removing YAP function in SCs. Mice with a conditional allele of the YAP locus (Zhang et al., 2010), $YAP^{fl/fl}$, were crossed with Merlin conditional animals, $NF2^{fl/fl}$, to generate Merlin null animals with the loss of either one, NF2-/-YAP+/-, or both, NF2-/-YAP-/-, YAP alleles. Analysis of mice with a SC-specific deletion of YAP alone (NF2+/+YAP-/-) revealed no developmental abnormalities in the nerve as measured by transmission EM of sciatic nerve at P6 and P21 (Fig. S4 A-E) and injury experiments in these animals showed a recovery profile, as measured by SSI analysis, indistinguishable from control wild-type animals (Fig. S4 G). Proliferation following injury at 7d showed no change in the numbers of Ki67 positive proliferating SCs or numbers of Iba1-positive macrophages recruited to the nerve in YAP-/- single null animals (Fig. S4 F, H). Both NF2-/-YAP+/- and NF2-/-YAP-/- animals were phenotypically normal and analysis of adult intact nerve in these animals revealed no abnormalities in axon number, diameter, or myelination by G ratio analysis and western blotting (Figs. S5 A-F and 9 F). Functional testing of mice by rotarod analysis showed no differences between adult NF2+/+YAP+/+, NF2-/-YAP+/+ and NF2-/-YAP-/- animals (Fig. S5 G.)

As described above and previously (Denisenko et al., 2008), loss of Merlin in SCs causes both a shortening of the internodal distance in the adult nerve, increased numbers of SCs and increased numbers of Schmidt-Lanterman incisures within myelinated SCs. Analysis of NF2-/-YAP+/- and NF2-/-YAP-/- adult P60 nerves showed that these three phenotypes were all corrected by the loss of YAP function in intact adult Merlin null nerves (Fig. S5 L-N.)

Western blotting of NF2+/+YAP+/+, NF2-/-YAP+/+ and NF2-/-YAP-/- nerves at 11d post-crush injury showed the loss of YAP induction in NF2-/-YAP-/- animals, confirming the SC-specificity of YAP induction in Merlin null (NF2-/-YAP+/+) nerves following injury (Fig. 8 G).

Next, we performed sciatic nerve crush injury experiments and assessment of recovery in NF2+/+YAP+/+, NF2-/-YAP+/+, NF2-/-YAP+/- and NF2-/-YAP-/- animals.

Remarkably, loss of even one copy of YAP in the NF2-/-YAP+/- animals was sufficient to restore some axonal regeneration and remyelination compared to the Merlin null (NF2-/-YAP+/+) animals at 21d post-crush injury. Loss of the second YAP allele in NF2-/-YAP-/- animals further restored axonal regeneration and numbers of myelinated fibres within the distal nerve (Fig. 7 A-D and F). Neurofilament staining in the distal sciatic nerve at 7d following crush injury showed increased numbers of regenerating axons in both NF2-/-YAP+/- and NF2-/-YAP-/- animals as compared to NF2-/-YAP+/+ animals even at this early timepoint following injury (Fig. 7 G-J). At 60d, there was a further improvement of regeneration in NF2-/-YAP-/- animals compared to 21d with larger numbers of myelinated axons present within the distal sciatic nerve (Fig. 7 F).

As above, mice with SC-specific loss of Merlin failed to recover by 21d as measured by SSI analysis (Fig. 5 A). In accordance with the axon regeneration and numbers of myelinated fibres in the distal nerve, loss of even one YAP allele in NF2-/-YAP+/- animals almost completely restored functional recovery by this measure in animals at 21d; loss of the second YAP allele (NF2-/-YAP-/-) led to complete functional recovery at 21d by SSI analysis with a recovery profile indistinguishable from the control NF2+/+YAP+/+ animals (Fig. 7 E). Sensory recovery, as measured by the toe pinch test showed a slight delay, but all NF2-/-YAP-/- animals showed a full recovery by this test at 26d compared to 21d for control animals. Transmission EM showed increased myelin thickness and decreased G ratios, for regenerated axons in the NF2-/-YAP+/- and NF2-/-YAP-/- animals as compared to Merlin null (NF2-/-YAP+/+) nerves at 21d post-injury (Fig. 8 A-D, H, I).

However, it should be noted that while there is a restoration of axonal regeneration, remyelination and functional recovery with the loss of YAP in Merlin null SCs, we still observed some, but reduced, numbers of abnormalities such as increased numbers of collagen fibres, collagen wrapping by SCs and large numbers of SC processes within NF2-/-YAP-/- distal nerves at 21d following injury (Fig. 8 D-F).

To further examine the role of YAP in the phenotype of Merlin null animals, we examined SC proliferation and macrophage infiltration, both of which are elevated in Merlin null animals (Fig. 4 H-K), in NF2-/-YAP-/- animals following crush injury. We found that loss of YAP reduced both the elevated cell proliferation and macrophage influx seen in Merlin null animals to that seen in control (NF2+/+YAP+/+) animals at 7d post injury (Fig. 8 J, K); these findings once again underline the importance of YAP signalling on the phenotype observed in Merlin null animals.

cJun and neurotrophin expression are reduced in Merlin null nerves following injury in a YAP-dependent manner.

The analysis of mice with SC-specific deletion of cJun has previously identified a reduced expression of the neurotrophins brain derived neurotrophic factor, BDNF, glial cell line-derived neurotrophic factor, GDNF, and artemin; administration of GDNF or artemin was shown to significantly improve the axon regeneration defect in cJun null animals (Arthur-Farraj et al., 2012; Fontana et al., 2012). Given that we observed a reduced induction of cJun in Merlin null nerves, we tested for mRNA and protein levels of cJun and these neurotrophins following injury. At 4 days post-crush injury, we observed a significant reduction in mRNA levels for cJun, BDNF, GDNF and artemin in Merlin null nerves as compared to controls. In all cases, these changes were partially reversed in Merlin/YAP double null animals (Fig. 9 A-D). These findings clearly identify for the first time that Merlin either directly or indirectly controls cJun expression *in vivo* in SCs following injury in a YAP-dependent manner. The partial restoration of cJun expression, together with the reduction in ERK1/2 activation, following injury in Merlin/YAP double null animals was also confirmed by western blotting (Fig. 9 E). In addition, an increase in TAZ protein was also observed in Merlin/YAP double null nerves following injury (Figs. 8 G and 9 E). In keeping with the normalised macrophage numbers seen in Merlin/YAP double null nerves following injury (Fig. 8 K), lower levels of MCP1 were observed in these nerves compared to Merlin null nerves (Fig. 9 E).

Finally to check the direct relationship between YAP expression and cJun expression, rat SCs were infected with adenovirus expressing either LacZ as a control or the non-phosphorylatable constitutively active FLAG-tagged $YAP^{Ser127Ala}$ (Shao et al., 2014) and levels of cJun protein measured. Immunolabelling of infected SCs showed

both nuclear and cytoplasmic localisation of the $YAP^{Ser127Ala}$ protein (Fig. 9 I and S5 O, P). We found that expression of $YAP^{Ser127Ala}$ alone was sufficient to lower cJun protein levels in rat SCs (Fig. 9 G-J).

These findings clearly identify that following PNS injury, Merlin-dependent signalling controls the correct up-regulation of cJun in SCs, together with neurotrophin expression, to ensure efficient axonal regeneration and functional repair. Loss of Merlin and consequent activation of YAP function in SCs suppresses this part of the regenerative response, leading to a failure of repair in the nerve following injury.

Discussion.

We have examined the consequences of Merlin loss upon the regenerative capacity of SCs in the peripheral nervous system following injury. In this system, SCs adopt, by cellular reprogramming, a repair-specific phenotype following injury that is required for the full axonal regeneration and the functional repair that can occur in this tissue (Arthur-Farraj et al., 2012; Jessen and Mirsky, 2016; Jessen et al., 2015). Given the multiple functions of the Merlin protein, it was somewhat surprising that loss of Merlin in SCs developmentally has only minor consequences in the development of the post-natal and adult nerve but, highlighting the potential differences between development and repair in the PNS, loss of Merlin in SCs causes the almost complete failure of repair following injury.

Following injury in Merlin null nerves we observe an increase in SC proliferation, an inhibition of axonal regeneration and a failure of SCs to correctly re-myelinate the few large diameter axons that do regenerate. In addition to this we observe an ongoing inflammatory state with increased numbers of macrophages within the nerve. It is interesting that these features are also characteristic of human schwannoma tumours in patients with NF2 (de Vries et al., 2013) and the possibility of local nerve compression or small injury as a trigger for such tumour formation is possibly consistent with the sites of such tumours on the 8th cranial nerve and at the spinal nerve roots of the PNS (Asthagiri et al., 2009; Hilton and Hanemann, 2014). Our analysis of the histology of distal Merlin null nerves at either 60 days or 8 months after injury indicates that they do show similarities to cellular schwannomas, but we have not observed the hallmark signs of human schwannoma such as Antoni type A or B regions or Verocay bodies in our experiments (Hilton and Hanemann, 2014) (Fig. S2 K, L and unpublished data).

Previous work in both transgenic knockout and older animals has identified the cJun transcription factor as a key protein in the generation of the repair-competent SC, or Büngner cell, in the distal nerve following injury (Arthur-Farraj et al., 2012; Painter et al., 2014; Parkinson et al., 2008) and we find that the up-regulation of cJun is delayed in Merlin null nerves, however we do not observe the block in myelin protein down-regulation or the reduced recruitment of macrophages seen in cJun null animals. It is unclear as to how much of a role this lack of myelin clearance plays in the reduced axonal regeneration seen in the cJun null nerves, but other work has shown that increased myelin debris seen following injury in aged animals causes stalling of motor axon re-growth in the PNS (Kang and Lichtman, 2013). The apparently normal myelin clearance we observe in Merlin null nerves would seemingly exclude this as a reason for the very poor regeneration of axons in our experiments. This, together with the altered cell proliferation and immune response we observe highlights clear differences between the SC cJun and Merlin null phenotypes following injury.

One possible explanation for the normal myelin clearance in Merlin null nerves is that we also observe increased activation of both ERK1/2 and p38 pathways following injury in Merlin null animals; both pathways have been shown to regulate SC demyelination and macrophage recruitment and it is unclear whether the effect of either MAPK is cJun dependent *in vivo* (Fischer et al., 2008b; Harrisingh et al., 2004; Napoli et al., 2012; Yang et al., 2012). It is possible that increased activation of these MAPK pathways, together with increased macrophage numbers, may compensate for the reduced induction of cJun in regulating these events of Wallerian degeneration. While the loss of axonal regeneration in Merlin null nerves may be cJun-dependent, both the increased SC proliferation and the inability to re-myelinate

the few regenerating axons following injury we observe are not apparent in cJun null animals (Arthur-Farraj et al., 2012). The increased severity of the regeneration defect seen in Merlin null nerves indicates other targets of Merlin and YAP-dependent signalling in controlling these processes.

Other phenotypes observed in the Merlin null nerves following injury, such as the wrapping of collagen fibres by SCs are not observed in cJun null nerves, but have been seen in mice with SC-specific loss of the phosphatase and tensin homologue (PTEN), with resulting increased PI3-kinase activity, and in mice expressing an activated form of Akt in SCs (Domenech-Estevez et al., 2016; Goebbels et al., 2010; Goebbels et al., 2012). Levels of p-Akt are increased in Merlin null nerves following injury (Fig. 9 E), in keeping with the increased PI-3 kinase/Akt signalling that has been shown in human Merlin null schwannoma cells in vitro (Ammoun et al., 2008). However, although this increased signalling through the PI3-kinase pathway may underlie the collagen wrapping by SCs and, perhaps, the increased deposition of basal lamina components (eg. collagen type IV, Fig. 6 D) in Merlin null nerves following injury (Domenech-Estevez et al., 2016), we clearly do not see the hypermyelination of axons seen in the PNS of these mouse PTEN mutants or Akt over-expressing nerves either before or following injury in the Merlin null nerves; indeed, we observe thinner re-myelination of the few larger diameter axons that do regenerate following injury (Fig. 3 G, H). Loss of YAP in Merlin null nerves appears to reduce levels of p-Akt following injury to those seen in control nerves (Fig. 9 E) and is associated with an improved re-myelination of regenerating axons. One possible mechanism for this effect upon Akt activity is that YAP has been shown to down-regulate levels of PTEN protein by inducing the microRNA miR-29 that inhibits PTEN mRNA translation in cells (Tumaneng et al., 2012).

The cause of the increased collagen fibres seen in Merlin null nerves following injury (Figs. 3 B, D, I and J and S2 I, J) is not clear but recent data, using a mouse transgenic expressing a constitutively active Mek1 (Mek1DD), has shown that increased ERK1/2 activity in SCs is associated with increased collagen fibre deposition in the intact adult peripheral nerve (Ishii et al., 2016). Thus, it is possible that the increased ERK1/2 activity in Merlin null nerves following injury (Fig. 6 C, D) drives a similar increase in collagen fibres within the nerve seen in our experiments.

Signalling through the Hippo pathway regulates multiple facets of cell behaviour, including cell proliferation, cell fate and ultimately tissue homeostasis and organ size (Yu et al., 2015). Regulation of the Hippo pathway by the Merlin protein has similarly been highly studied in the control of cell behaviour in tumours with the loss of Merlin function and in particular schwannomas and meningiomas of the nervous system (Asthagiri et al., 2009; Cooper and Giancotti, 2014; Li et al., 2014). While the increase expression of YAP following injury is only seen in Merlin null nerves, increased TAZ expression following injury is also seen in control nerves. Such a differential expression of YAP and TAZ has also been observed in the dorsal horn following nerve injury as well as in hepatocellular carcinoma tumours, highlighting potentially different roles for YAP and TAZ proteins in these situations (Hayashi et al., 2015; Xu et al., 2016). It remains to be determined whether there are distinct roles for these two Hippo pathway effectors in SCs in the events of nerve repair.

YAP null nerves show no developmental defects and no defects in repair (Fig. S4 A-H), whereas TAZ null nerves show some defects in axonal sorting (Poitelon et al., 2016 and our unpublished data). Recent work has shown that absence of both YAP and TAZ in SCs during development causes a severe peripheral neuropathy due to defects in axonal sorting and that YAP/TAZ-dependent transcription regulates

laminin receptors in SCs (Poitelon et al., 2016). The effects of TAZ loss alone in SCs upon PNS repair and whether loss of TAZ function will revert part or all of the phenotype of Merlin null nerves following injury remains to be tested.

In conclusion, we have identified a completely novel function for the Merlin tumour suppressor in the control of SC reprogramming and PNS repair following injury. The finding that increased expression of YAP in Merlin null nerves blocks the regenerative capacity of SCs to accomplish repair also demonstrates a new function for the Hippo/YAP pathway in this phenotype of Merlin null nerves. These findings identify a potential novel mechanism for situations in which SCs may not be fully supportive and nerve repair may not be optimal, such as diabetic neuropathy, in the aging nerve (Painter et al., 2014) or situations that lead to longer term denervation of the distal nerve (Dahlin, 2013). Targeting of YAP-dependent signalling in such circumstances may, perhaps, offer an improvement in functional repair and outcome.

Acknowledgements.

This work was supported by grants from the UK Medical Research Council (Ref. MR/J012785/1) and the Northcott Devon Medical Foundation (ref. TB/MG/NO5002) to D.B.P. We are grateful for excellent technical support from Dr. R. Moate, Mr P. Bond and Mr G. Harper in the Plymouth University EM Centre for help with EM processing and imaging. We thank Profs L. Feltri and L. Wrabetz (Univ. of New York at Buffalo, USA) for providing the P0-CRE mice and Prof. Marco Giovannini (UCLA, USA) for the conditional NF2 mice. We are grateful to Profs R. Mirsky and K.R. Jessen (UCL, UK) for comments on the manuscript. We thank Dr S. Ikeda and Prof. J. Sadoshima (Rutgers Univ., USA) for the LacZ and YAP-expressing adenoviruses, Dr W.A. Woldie for help with quantitative PCR and Mr W.Woznica for excellent technical support with animal husbandry.

Author Contributions.

T.M., X-P.D, K.N, R.D.S.D, S.R, A.S, J.R., G.M. and D.B.P. designed experiments and analysed data. B.G, P.E. and A.S. performed experiments and analysed data. N.Z. and D.P. provided transgenic mice and experimental guidance. T.M., H.M. and D.B.P. wrote and edited the manuscript.

Competing Financial Interests.

The authors declare no competing financial interests.

References.

Ammoun, S., C. Flaiz, N. Ristic, J. Schuldt, and C.O. Hanemann. 2008. Dissecting and targeting the growth factor-dependent and growth factor-independent extracellular signal-regulated kinase pathway in human schwannoma. *Cancer Res*. 68:5236-5245.

Arthur-Farraj, P.J., M. Latouche, D.K. Wilton, S. Quintes, E. Chabrol, A. Banerjee, A. Woodhoo, B. Jenkins, M. Rahman, M. Turmaine, G.K. Wicher, R. Mitter, L. Greensmith, A. Behrens, G. Raivich, R. Mirsky, and K.R. Jessen. 2012. c-Jun Reprograms Schwann Cells of Injured Nerves to Generate a Repair Cell Essential for Regeneration. *Neuron*. 75:633-647.

Asthagiri, A.R., D.M. Parry, J.A. Butman, H.J. Kim, E.T. Tsilou, Z. Zhuang, and R.R. Lonser. 2009. Neurofibromatosis type 2. *Lancet*. 373:1974-1986.

Baptista, A.F., J.R. Gomes, J.T. Oliveira, S.M. Santos, M.A. Vannier-Santos, and A.M. Martinez. 2007. A new approach to assess function after sciatic nerve lesion in the mouse - adaptation of the sciatic static index. *J Neurosci Methods*. 161:259-264.

Cooper, J., and F.G. Giancotti. 2014. Molecular insights into NF2/Merlin tumor suppressor function. *FEBS Lett*.

Crawford, A.T., D. Desai, P. Gokina, S. Basak, and H.A. Kim. 2008. E-cadherin expression in postnatal Schwann cells is regulated by the cAMP-dependent protein kinase a pathway. *Glia*. 56:1637-1647.

Dahlin, L.B. 2013. The role of timing in nerve reconstruction. *Int Rev Neurobiol*. 109:151-164.

de Vries, M., I. Briaire-de Bruijn, M.J. Malessy, S.F. de Bruine, A.G. van der Mey, and P.C. Hogendoorn. 2013. Tumor-associated macrophages are related to volumetric growth of vestibular schwannomas. *Otol Neurotol*. 34:347-352.

Denisenko, N., C. Cifuentes-Diaz, T. Irinopoulou, M. Carnaud, E. Benoit, M. Niwa-Kawakita, F. Chareyre, M. Giovannini, J.A. Girault, and L. Goutebroze. 2008. Tumor suppressor schwannomin/merlin is critical for the organization of Schwann cell contacts in peripheral nerves. *J Neurosci*. 28:10472-10481.

Doddrell, R.D., X.P. Dun, A. Shivane, M.L. Feltri, L. Wrabetz, M. Wegner, E. Sock, C.O. Hanemann, and D.B. Parkinson. 2013. Loss of SOX10 function contributes to the phenotype of human Merlin-null schwannoma cells. *Brain*. 136:549-563.

Domenech-Estevez, E., H. Baloui, X. Meng, Y. Zhang, K. Deinhardt, J.L. Dupree, S. Einheber, R. Chrast, and J.L. Salzer. 2016. Akt Regulates Axon Wrapping and Myelin Sheath Thickness in the PNS. *J Neurosci*. 36:4506-4521.

Dun, X.P., and D.B. Parkinson. 2015. Visualizing peripheral nerve regeneration by whole mount staining. *PLoS One*. 10:e0119168.

Feltri, M.L., M. D'Antonio, S. Previtali, M. Fasolini, A. Messing, and L. Wrabetz. 1999. P0-Cre transgenic mice for inactivation of adhesion molecules in Schwann cells. *Ann N Y Acad Sci*. 883:116-123.

Fey, A., M. Schachner, and A. Irintchev. 2010. A novel motion analysis approach reveals late recovery in C57BL/6 mice and deficits in NCAM-deficient mice after sciatic nerve crush. *Journal of neurotrauma*. 27:815-828.

Fischer, S., C. Kleinschnitz, M. Muller, I. Kobsar, C.W. Ip, B. Rollins, and R. Martini. 2008a. Monocyte chemoattractant protein-1 is a pathogenic component in a model for a hereditary peripheral neuropathy. *Mol Cell Neurosci*. 37:359-366.

Fischer, S., A. Weishaupt, J. Troppmair, and R. Martini. 2008b. Increase of MCP-1 (CCL2) in myelin mutant Schwann cells is mediated by MEK-ERK signaling pathway. *Glia*. 56:836-843.

Fontana, X., M. Hristova, C. Da Costa, S. Patodia, L. Thei, M. Makwana, B. Spencer-Dene, M. Latouche, R. Mirsky, K.R. Jessen, R. Klein, G. Raivich, and A. Behrens. 2012. c-Jun in Schwann cells promotes axonal regeneration and motoneuron survival via paracrine signaling. *J Cell Biol*. 198:127-141.

Gehlhausen, J.R., S.J. Park, A.E. Hickox, M. Shew, K. Staser, S.D. Rhodes, K. Menon, J.D. Lajiness, M. Mwanthi, X. Yang, J. Yuan, P. Territo, G. Hutchins, G. Nalepa, F.C. Yang, S.J. Conway, M.G. Heinz, A. Stemmer-Rachamimov, C.W. Yates, and D. Wade Clapp. 2015. A murine model of neurofibromatosis type 2 that accurately phenocopies human schwannoma formation. *Hum Mol Genet*. 24:1-8.

Giovannini, M., E. Robanus-Maandag, M. van der Valk, M. Niwa-Kawakita, V. Abramowski, L. Goutebroze, J.M. Woodruff, A. Berns, and G. Thomas. 2000. Conditional biallelic Nf2 mutation in the mouse promotes manifestations of human neurofibromatosis type 2. *Genes Dev*. 14:1617-1630.

Goebbels, S., J.H. Oltrogge, R. Kemper, I. Heilmann, I. Bormuth, S. Wolfer, S.P. Wichert, W. Mobius, X. Liu, C. Lappe-Siefke, M.J. Rossner, M. Groszer, U. Suter, J. Frahm, S. Boretius, and K.A. Nave. 2010. Elevated phosphatidylinositol 3,4,5-trisphosphate in glia triggers cell-autonomous membrane wrapping and myelination. *J Neurosci*. 30:8953-8964.

Goebbels, S., J.H. Oltrogge, S. Wolfer, G.L. Wieser, T. Nientiedt, A. Pieper, T. Ruhwedel, M. Groszer, M.W. Sereda, and K.A. Nave. 2012. Genetic

disruption of Pten in a novel mouse model of tomaculous neuropathy. *EMBO Mol Med*. 4:486-499.

Hanemann, C.O. 2008. Magic but treatable? Tumours due to loss of merlin. *Brain*. 131:606-615.

Harrisingh, M.C., E. Perez-Nadales, D.B. Parkinson, D.S. Malcolm, A.W. Mudge, and A.C. Lloyd. 2004. The Ras/Raf/ERK signalling pathway drives Schwann cell dedifferentiation. *EMBO J*. 23:3061-3071.

Hayashi, H., T. Higashi, N. Yokoyama, T. Kaida, K. Sakamoto, Y. Fukushima, T. Ishimoto, H. Kuroki, H. Nitta, D. Hashimoto, A. Chikamoto, E. Oki, T. Beppu, and H. Baba. 2015. An Imbalance in TAZ and YAP Expression in Hepatocellular Carcinoma Confers Cancer Stem Cell-like Behaviors Contributing to Disease Progression. *Cancer Res*. 75:4985-4997.

Hilton, D.A., and C.O. Hanemann. 2014. Schwannomas and their pathogenesis. *Brain Pathol*. 24:205-220.

Ishii, A., M. Furusho, J.L. Dupree, and R. Bansal. 2016. Strength of ERK1/2 MAPK Activation Determines Its Effect on Myelin and Axonal Integrity in the Adult CNS. *J Neurosci*. 36:6471-6487.

Jessen, K.R., and R. Mirsky. 2016. The repair Schwann cell and its function in regenerating nerves. *J Physiol*.

Jessen, K.R., R. Mirsky, and P. Arthur-Farraj. 2015. The Role of Cell Plasticity in Tissue Repair: Adaptive Cellular Reprogramming. *Dev Cell*. 34:613-620.

Kang, H., and J.W. Lichtman. 2013. Motor axon regeneration and muscle reinnervation in young adult and aged animals. *J Neurosci*. 33:19480-19491.

Kim, H.A., T. Mindos, and D.B. Parkinson. 2013. Plastic fantastic: Schwann cells and repair of the peripheral nervous system. *Stem cells translational medicine*. 2:553-557.

Kuhn, P.L., E. Petroulakis, G.A. Zazanis, and R.D. McKinnon. 1995. Motor function analysis of myelin mutant mice using a rotarod. *International Journal of Developmental Neuroscience*. 13:715-722.

Li, W., J. Cooper, L. Zhou, C. Yang, H. Erdjument-Bromage, D. Zagzag, M. Snuderl, M. Ladanyi, C.O. Hanemann, P. Zhou, M.A. Karajannis, and F.G. Giancotti. 2014. Merlin/NF2 loss-driven tumorigenesis linked to CRL4(DCAF1)-mediated inhibition of the hippo pathway kinases Lats1 and 2 in the nucleus. *Cancer Cell*. 26:48-60.

Myers, R.R., Y. Sekiguchi, S. Kikuchi, B. Scott, S. Medicherla, A. Protter, and W.M. Campana. 2003. Inhibition of p38 MAP kinase activity enhances axonal regeneration. *Exp Neurol*. 184:606-614.

Napoli, I., L.A. Noon, S. Ribeiro, A.P. Kerai, S. Parrinello, L.H. Rosenberg, M.J. Collins, M.C. Harrisingh, I.J. White, A. Woodhoo, and A.C. Lloyd. 2012. A central role for the ERK-signaling pathway in controlling Schwann cell plasticity and peripheral nerve regeneration in vivo. *Neuron*. 73:729-742.

Painter, M.W., A. Brosius Lutz, Y.C. Cheng, A. Latremoliere, K. Duong, C.M. Miller, S. Posada, E.J. Cobos, A.X. Zhang, A.J. Wagers, L.A. Havton, B. Barres, T. Omura, and C.J. Woolf. 2014. Diminished Schwann cell repair responses underlie age-associated impaired axonal regeneration. *Neuron*. 83:331-343.

Parkinson, D.B., A. Bhaskaran, P. Arthur-Farraj, L.A. Noon, A. Woodhoo, A.C. Lloyd, M.L. Feltri, L. Wrabetz, A. Behrens, R. Mirsky, and K.R. Jessen. 2008. c-Jun is a negative regulator of myelination. *J Cell Biol*. 181:625-637.

Parkinson, D.B., A. Bhaskaran, A. Droggiti, S. Dickinson, M. D'Antonio, R. Mirsky, and K.R. Jessen. 2004. Krox-20 inhibits Jun-NH2-terminal kinase/c-Jun to control Schwann cell proliferation and death. *J Cell Biol*. 164:385-394.

Parkinson, D.B., S. Dickinson, A. Bhaskaran, M.T. Kinsella, P.J. Brophy, D.L. Sherman, S. Sharghi-Namini, M.B. Duran Alonso, R. Mirsky, and K.R. Jessen. 2003. Regulation of the myelin gene periaxin provides evidence for Krox-20-independent myelin-related signalling in Schwann cells. *Mol Cell Neurosci*. 23:13-27.

Poitelon, Y., C. Lopez-Anido, K. Catignas, C. Berti, M. Palmisano, C. Williamson, D. Ameroso, K. Abiko, Y. Hwang, A. Gregorieff, J.L. Wrana, M. Asmani, R. Zhao, F.J. Sim, L. Wrabetz, J. Svaren, and M.L. Feltri. 2016. YAP and TAZ control peripheral myelination and the expression of laminin receptors in Schwann cells. *Nat Neurosci*. 19:879-887.

Pratt-Hyatt, M., A.J. Lickteig, and C.D. Klaassen. 2013. Tissue distribution, ontogeny, and chemical induction of aldo-keto reductases in mice. *Drug Metab Dispos*. 41:1480-1487.

Schulz, A., S.L. Baader, M. Niwa-Kawakita, M.J. Jung, R. Bauer, C. Garcia, A. Zoch, S. Schacke, C. Hagel, V.F. Mautner, C.O. Hanemann, X.P. Dun, D.B. Parkinson, J. Weis, J.M. Schroder, D.H. Gutmann, M. Giovannini, and H. Morrison. 2013. Merlin isoform 2 in neurofibromatosis type 2-associated polyneuropathy. *Nat Neurosci*. 16:426-433.

Schulz, A., R. Buttner, C. Hagel, S.L. Baader, L. Kluwe, J. Salamon, V.F. Mautner, T. Mindos, D.B. Parkinson, J.R. Gehlhausen, D.W. Clapp, and H. Morrison. 2016. The importance of nerve microenvironment for schwannoma development. *Acta Neuropathol*.

Schulz, A., A. Kyselyova, S.L. Baader, M.J. Jung, A. Zoch, V.F. Mautner, C. Hagel, and H. Morrison. 2014a. Neuronal merlin influences ERBB2 receptor expression on Schwann cells through neuregulin 1 type III signalling. *Brain*. 137:420-432.

Schulz, A., C. Walther, H. Morrison, and R. Bauer. 2014b. In vivo electrophysiological measurements on mouse sciatic nerves. *J Vis Exp*.

Shao, D., P. Zhai, D.P. Del Re, S. Sciarretta, N. Yabuta, H. Nojima, D.S. Lim, D. Pan, and J. Sadoshima. 2014. A functional interaction between Hippo-YAP signalling and FoxO1 mediates the oxidative stress response. *Nature communications*. 5:3315.

Sharghi-Namini, S., M. Turmaine, C. Meier, V. Sahni, F. Umehara, K.R. Jessen, and R. Mirsky. 2006. The structural and functional integrity of peripheral nerves depends on the glial-derived signal desert hedgehog. *J Neurosci*. 26:6364-6376.

Shimomura, T., N. Miyamura, S. Hata, R. Miura, J. Hirayama, and H. Nishina. 2014. The PDZ-binding motif of Yes-associated protein is required for its co-activation of TEAD-mediated CTGF transcription and oncogenic cell transforming activity. *Biochem Biophys Res Commun*. 443:917-923.

Tofaris, G.K., P.H. Patterson, K.R. Jessen, and R. Mirsky. 2002. Denervated Schwann cells attract macrophages by secretion of leukemia inhibitory factor (LIF) and monocyte chemoattractant protein-1 in a process regulated by interleukin-6 and LIF. *J Neurosci*. 22:6696-6703.

Truett, G.E., P. Heeger, R.L. Mynatt, A.A. Truett, J.A. Walker, and M.L. Warman. 2000. Preparation of PCR-quality mouse genomic DNA with hot sodium hydroxide and tris (HotSHOT). *Biotechniques*. 29:52, 54.

Tumaneng, K., K. Schlegelmilch, R.C. Russell, D. Yimlamai, H. Basnet, N. Mahadevan, J. Fitamant, N. Bardeesy, F.D. Camargo, and K.L. Guan. 2012. YAP mediates crosstalk between the Hippo and PI(3)K-TOR pathways by suppressing PTEN via miR-29. *Nat Cell Biol*. 14:1322-1329.

Xu, N., M.Z. Wu, X.T. Deng, P.C. Ma, Z.H. Li, L. Liang, M.F. Xia, D. Cui, D.D. He, Y. Zong, Z. Xie, and X.J. Song. 2016. Inhibition of YAP/TAZ Activity in Spinal Cord Suppresses Neuropathic Pain. *J Neurosci*. 36:10128-10140.

Yang, D.P., J. Kim, N. Syed, Y.J. Tung, A. Bhaskaran, T. Mindos, R. Mirsky, K.R. Jessen, P. Maurel, D.B. Parkinson, and H.A. Kim. 2012. p38 MAPK activation promotes denervated Schwann cell phenotype and functions as a negative regulator of Schwann cell differentiation and myelination. *J Neurosci*. 32:7158-7168.

Yang, D.P., D.P. Zhang, K.S. Mak, D.E. Bonder, S.L. Pomeroy, and H.A. Kim. 2008. Schwann cell proliferation during Wallerian degeneration is not necessary for regeneration and remyelination of the peripheral nerves: axon-dependent removal of newly generated Schwann cells by apoptosis. *Mol Cell Neurosci*. 38:80-88.

Yu, F.X., B. Zhao, and K.L. Guan. 2015. Hippo Pathway in Organ Size Control, Tissue Homeostasis, and Cancer. *Cell*. 163:811-828.

Zhang, N., H. Bai, K.K. David, J. Dong, Y. Zheng, J. Cai, M. Giovannini, P. Liu, R.A. Anders, and D. Pan. 2010. The Merlin/NF2 tumor suppressor functions through the YAP oncoprotein to regulate tissue homeostasis in mammals. *Dev Cell*. 19:27-38.

Zhao, B., L. Li, Q. Lei, and K.L. Guan. 2010. The Hippo-YAP pathway in organ size control and tumorigenesis: an updated version. *Genes Dev*. 24:862-874.

Figures and Figure Legends:

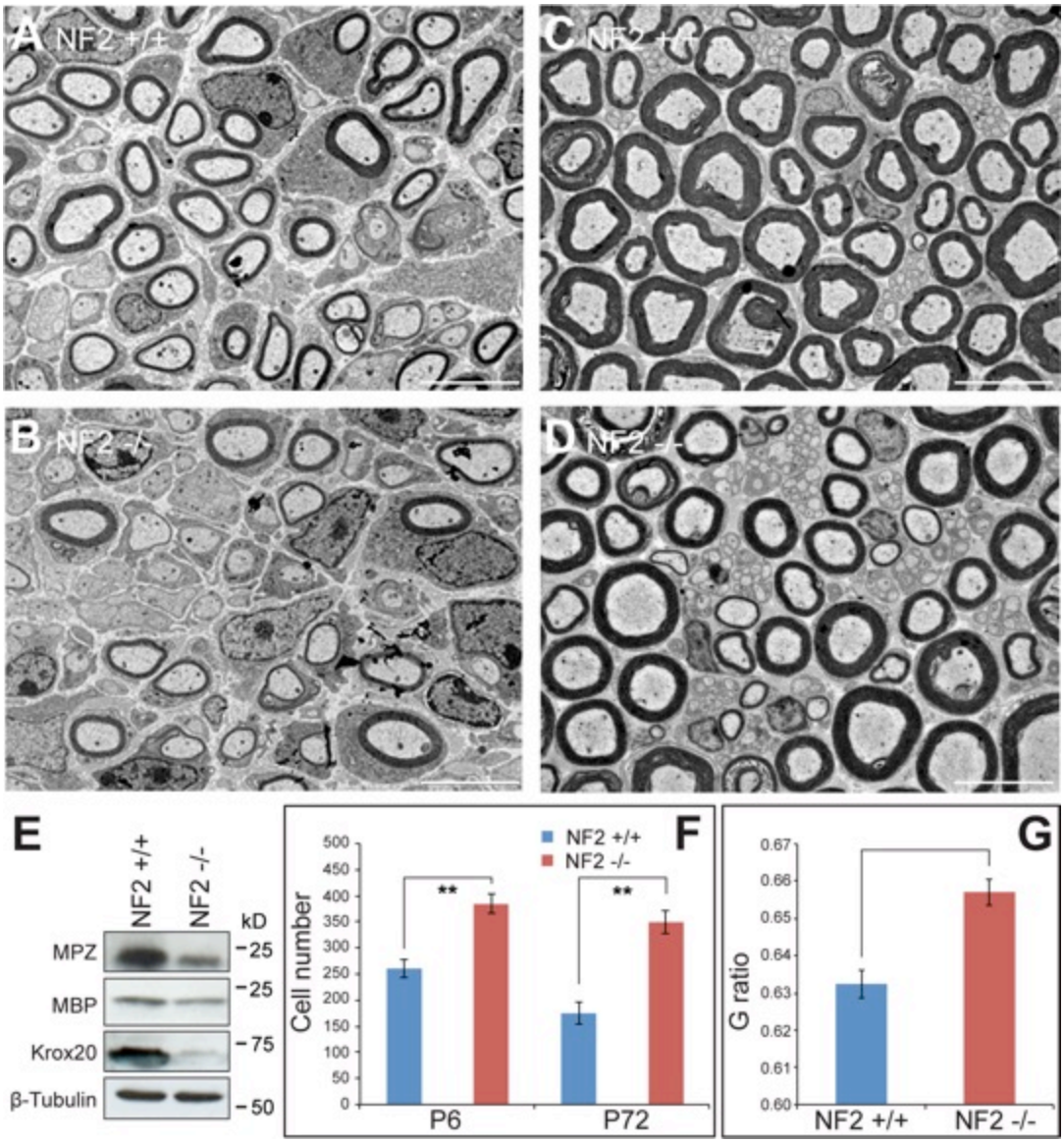

Figure 1: Merlin null nerves show a transient hypomyelination and slight increase in Schwann cell numbers. **A**, **B**. Transmission EM pictures of post-natal day (P) 6 sciatic nerves of control (NF2+/+, A) and Merlin null (NF2-/-, B) animals (n=3 mice). Scale bar 5µm. **C**, **D**. Transmission EM pictures of P60 sciatic nerve from control (C) and Merlin null (D) animals (n=3 mice). Scale bar 10µm. **E**. Western blot of control and Merlin null nerves at P6 (n=3 pools, 1 pool=3 nerves from 3 mice for each genotype). β-tubulin is used as loading control. **F**. Counts of Hoechst stained nuclei from transverse cryostat sections of P6 and P72 sciatic nerves showing increase in

cell number in Merlin null nerves; (NF2+/+ n=3, NF2-/- n=4). **G**. Small but non-significant increase in G ratio in P60 Merlin null nerves as compared to control (n=3 mice). Two-sided Two-Sample Student's *t* test $^{**}P \leq 0.004$ (P6, F), $^{**}P \leq 0.005$ (P72, F), $P=0.1$ (G).

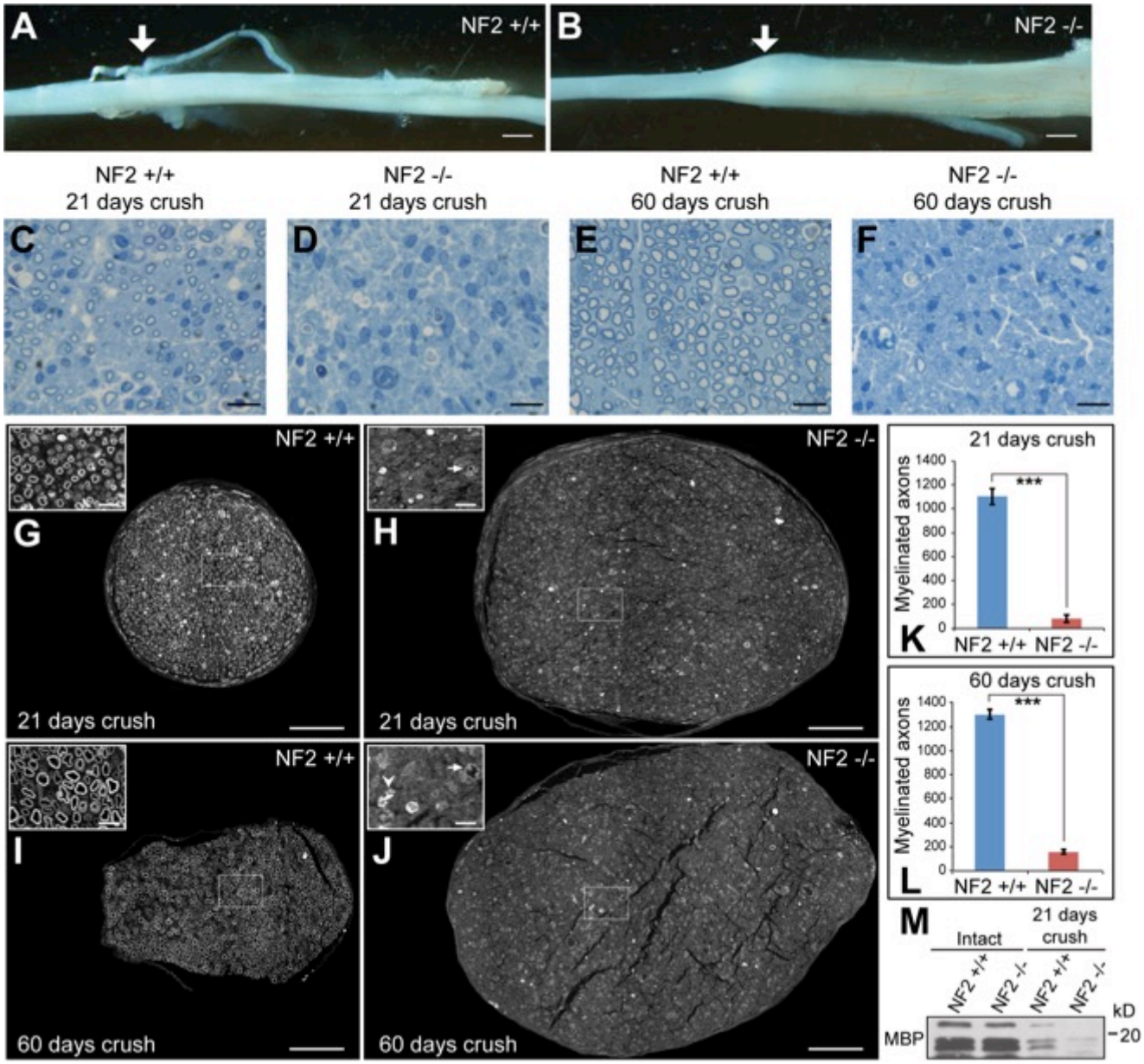

Figure 2: Loss of Merlin in Schwann cells causes a severe regeneration defect following injury. **A**, **B**. Phase photos showing sciatic nerve 21 days (d) after crush injury in control (NF2+/+, A) and Schwann cell-specific Merlin null (NF2-/-, B) nerves; white arrow marks the site of crush injury. There is a substantial expansion of the distal nerve in Merlin null nerves (observed in all analysed NF2-/- nerves following injury). Scale bar 2mm. **C-F**. Semi-thin sections of distal sciatic nerve at 21d (C, D) and 60d (E, F) post crush injury. Scale bar 50µm. **G-J**. Low vacuum scanning EM of control (G, I) and Merlin-null (H, J) tibial nerves at 21d and 60d post-crush injury;

insets show higher magnification images of the samples showing remyelination in control samples but almost no remyelination in Merlin null nerves. Arrows in inset in panels H and J show thinly remyelinated axons; arrowhead in inset in panel J shows presence of macrophages in the nerve at 60d (n=3 mice for each genotype and time point). Scale bar 50μm. Insets scale bar 25μm. **K**, **L**. Counts of numbers of myelinated fibres in tibial nerves at 21d (K) and 60d (L) post-crush injury with significantly fewer myelinated fibres in NF2-/- nerves at both timepoints (n=3 mice for each genotype and time point). **M**. Western blot of myelin basic protein (MBP) in intact and injured distal sciatic nerves 21d after nerve crush (n=3 mice for each genotype and time point). Two-sided Two-Sample Student's *t* test ***$P \leq 0.001$ in both time points (K, L).

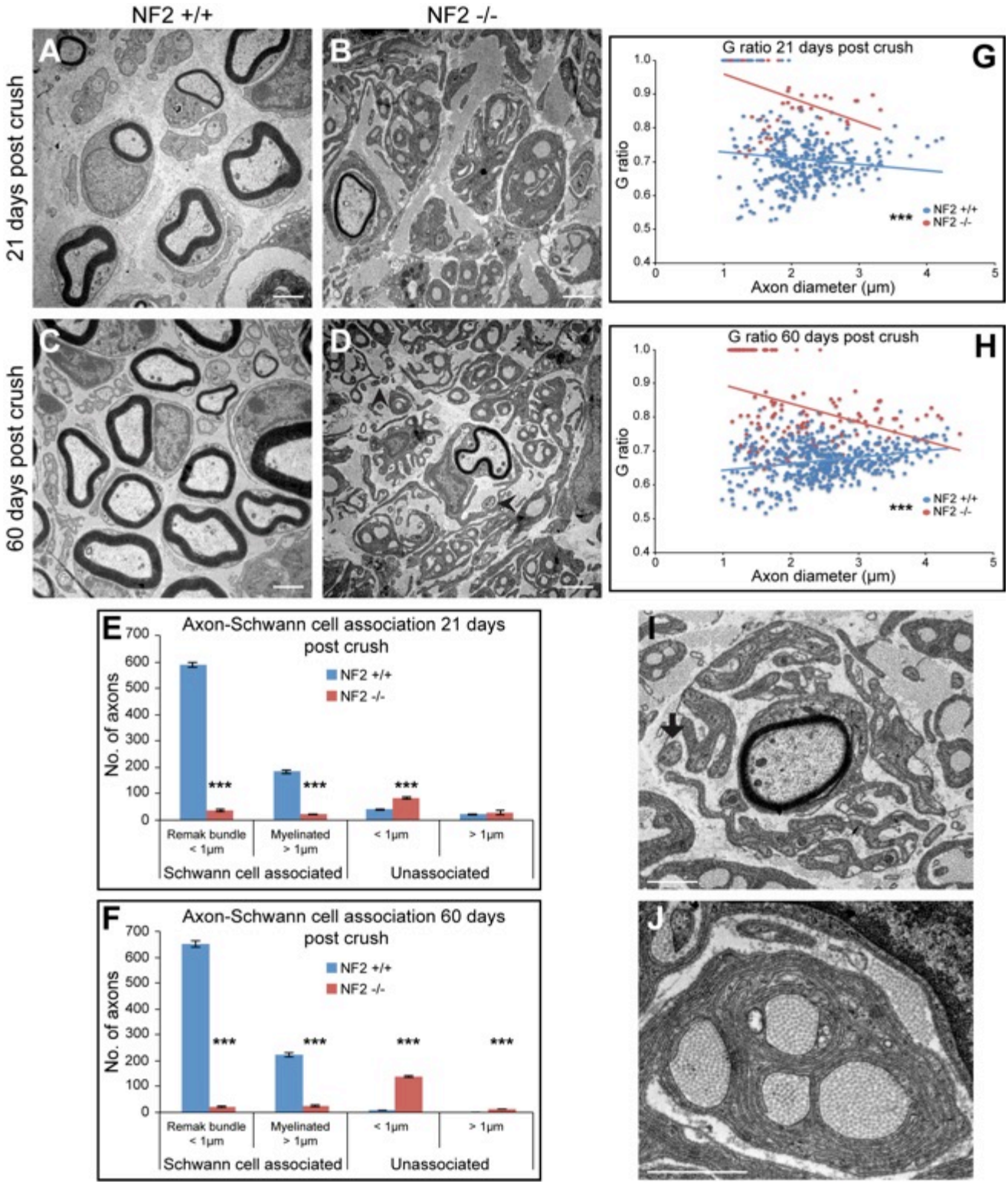

Figure 3: Remyelination and morphological analysis of control and Merlin-null nerves after injury. **A-D**. Transmission EM pictures of control (A, C; NF2+/+) and Merlin null (B, D; NF2-/-) distal sciatic nerves at 21d (A, B) and 60d (C, D) following nerve crush. Arrowheads in D indicate small diameter axons that are un-associated

with Schwann cells (n=3 mice). Scale bar 2μm. **E**, **F**. Counts of axons and Schwann cell-axon association in sciatic nerves of control and Merlin-null animals at 21d (E) and 60d (F) post-injury (n=3 mice), indicating poor association of Merlin null Schwann cells with both small (<1μm) and larger (>1μm) diameter axons and corresponding increased numbers of un-associated axons in these nerves post-injury. **G**, **H**. G-ratio vs axon diameter scatter plot graphs for control and Merlin null sciatic nerves at 21d (G) and 60d (H) post injury (n=3 mice). **I**, **J**. Transmission EM of Merlin null sciatic nerves at 60d post-injury showing large amounts of collagen fibres, extensive Schwann cell processes and large degree of collagen wrapping by Schwann cells within the nerve. Arrow in I indicates a small diameter axon that is un-associated with a Schwann cell and residing inside the discontinuous basal lamina of the myelinating Schwann cell. Notice in J the Schwann cell ensheaths the collagen fibres with multiple membrane bilayers. (Representative images from 3 biological replicates). Scale bar 1μm. Two-sided Two-Sample Student's *t* test *** $P \leq 0.001$ for all comparisons in Schwann cell-axon association graphs against the control NF2+/+ at both time points (E, F), $P = 0.464$ for un-associated axons >1μm (E), *** $P \leq 0.001$ for the G ratio at 21d and 60d post crush (G, H).

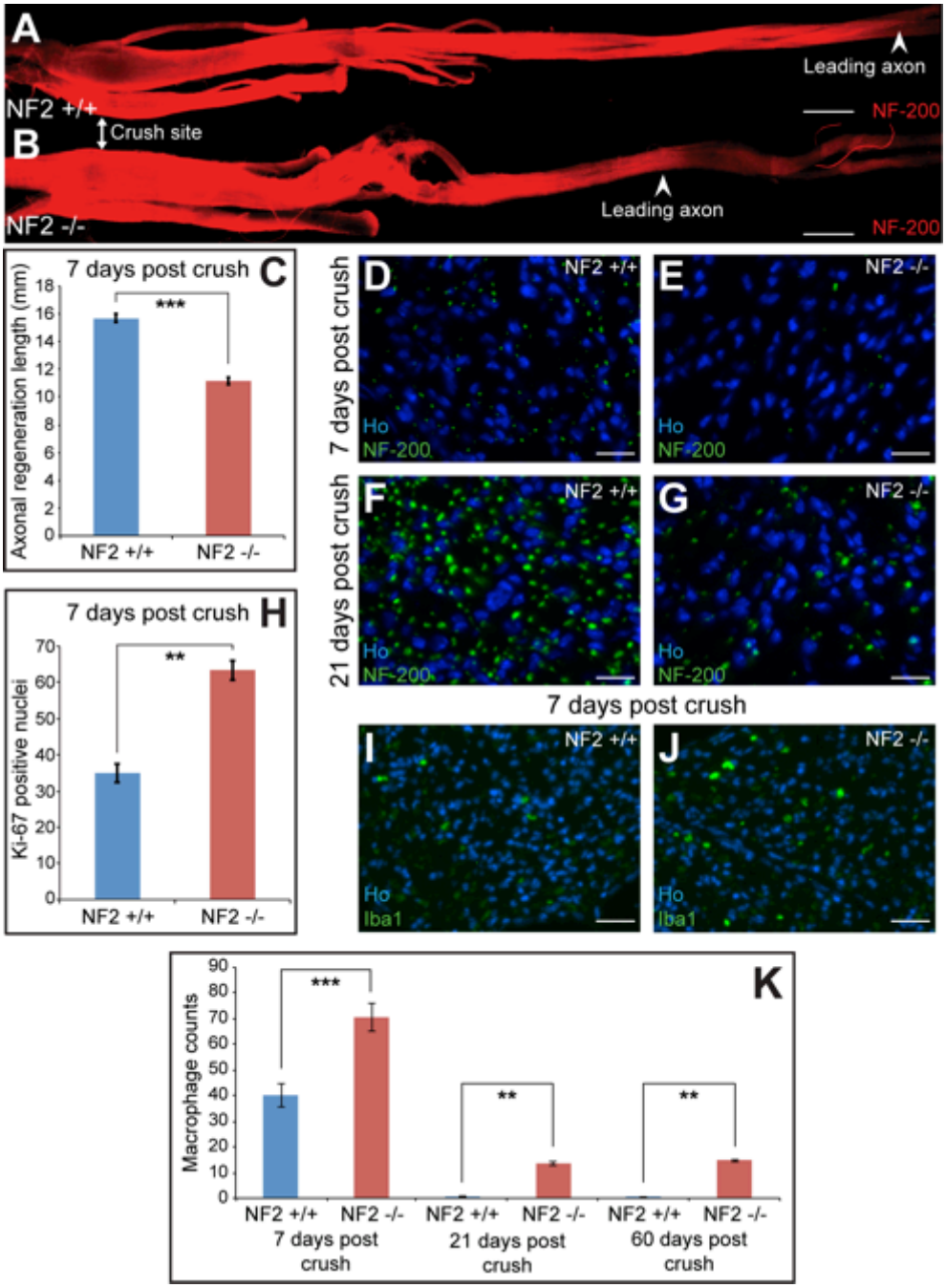

Figure 4: Loss of Merlin causes a failure in axonal regrowth and distal nerves are characterised by increased Schwann cell proliferation and ongoing presence of macrophages. **A, B**. Wholemount staining of control (NF2+/+) and Merlin null (NF2-/-) nerve at 7d after crush injury. Nerves are stained with neurofilament antibody (NF200), the crush site is marked, and arrowheads mark the leading regenerating axons in control and Merlin-null nerves. Scale bar 1mm. **C**. Quantification of distance

of leading axons relative to injury site at 7d post crush in control and Merlin null nerves (n= 3 mice). **D-G**. Immunolabelling with neurofilament antibody of distal sciatic nerve at 7d (D, E) and 21d (F, G) after nerve crush (n=3 mice). Scale bar 25μm. **H**. Increased Schwann cell proliferation, as measured by Ki67 labelling, in Merlin null distal sciatic nerve at 7d after crush injury (n=3 mice). **I-K**. Labelling (I, J) and quantification (K) of Iba1 positive macrophages in control and Merlin null sciatic nerves at 7d, 21d and 60d post crush injury (n=3 mice for each genotype and time point). I, J Scale bar 100μm. Two-sided Two-Sample Student's *t* test ***$P \leq 0.001$ (C), **$P \leq 0.01$ (H), **$P \leq 0.01$, ***$P \leq 0.001$ (K).

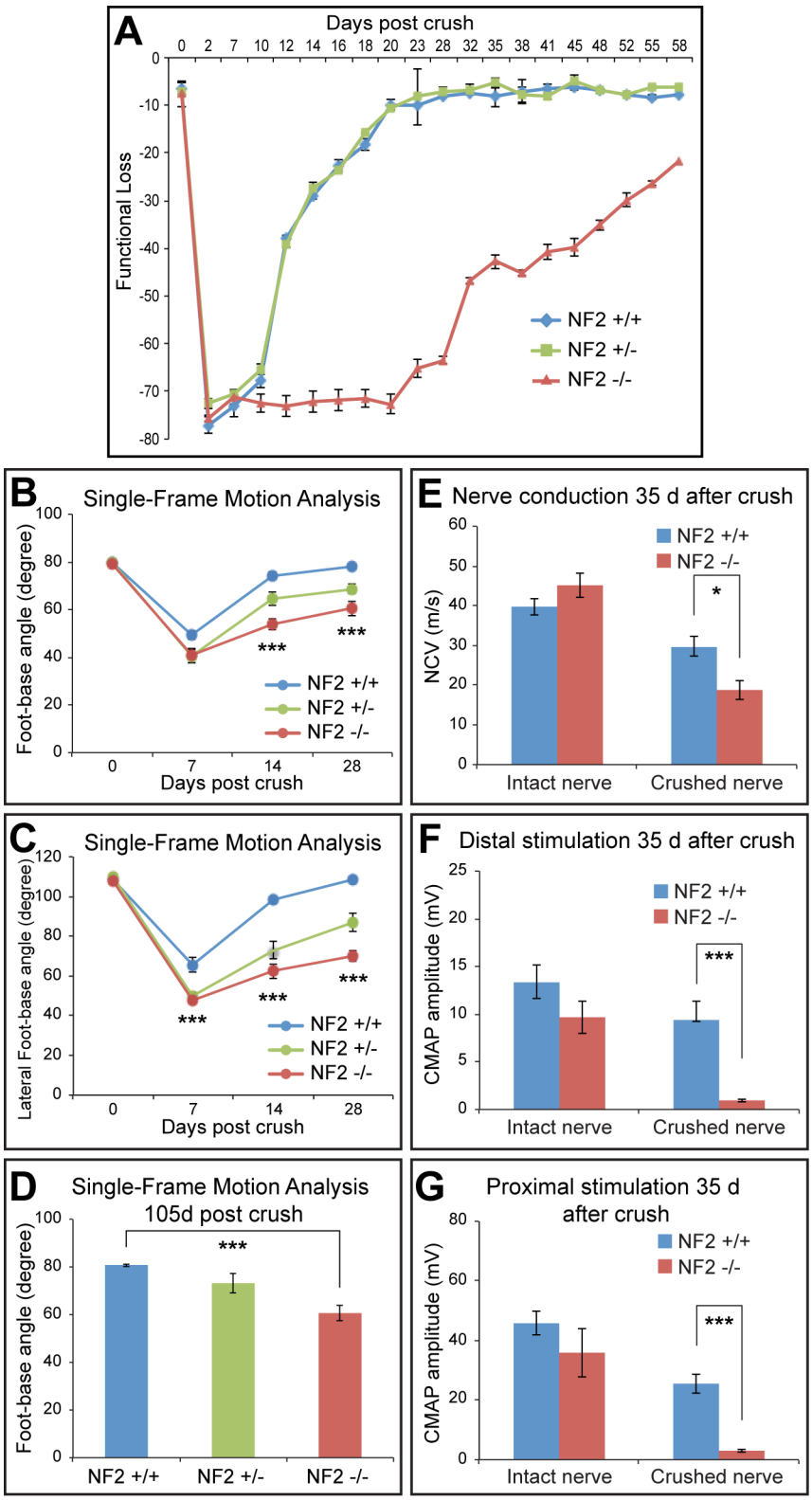

Figure 5: Merlin null animals display diminished functional recovery at all time points following injury. **A**. Static sciatic index (SSI) measurements of control (NF2+/+), heterozygous (NF2+/-) and Merlin null animals (NF2-/-) (n=3 mice for each time

point). **B-D**. Single frame motion analysis of animals for foot-base angle (B) and lateral foot-base angle (C) up to 28d after injury. D. Measurement of foot-base angle in animals at fifteen weeks (105d) post-crush injury (n=7 mice for each time point). **E**. Measurements of nerve conduction velocity (NCV) of control and Merlin null animals from contralateral control and side of nerve crush at 35d after crush injury (n=7 mice). **F**, **G**. Measurements of compound muscle action potential (CMAP) with distal (F) and proximal (G) stimulation (n=7 mice). One-way ANOVA with Bonferroni's multiple comparison test ***$P \leq 0.001$ for all time points compared to NF2+/+ (B-D). Two-sided Two-Sample Student's *t* test *$P = 0.014$ (E), ***$P \leq 0.001$ (F, G).

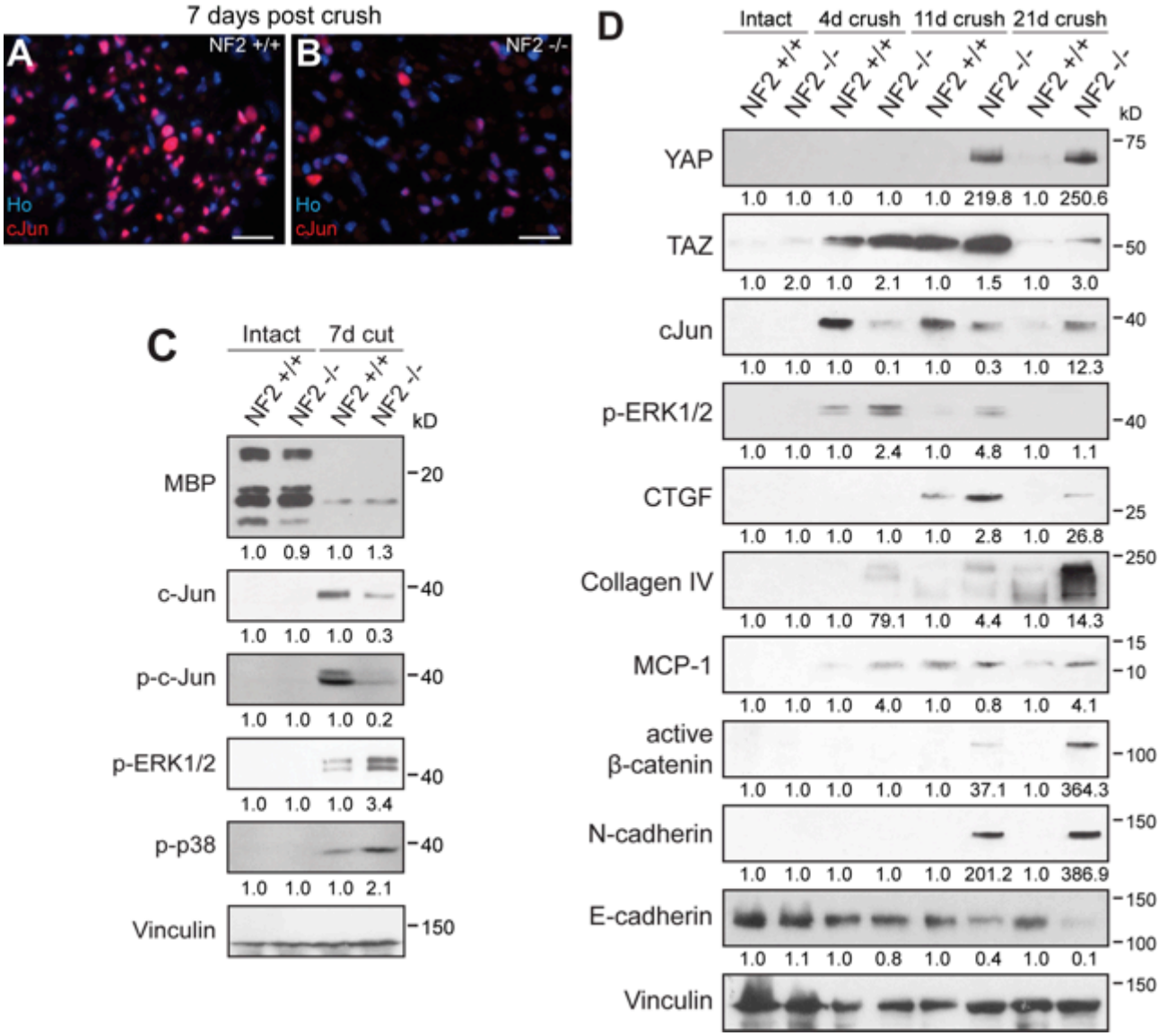

Figure 6: Merlin function in Schwann cells regulates cJun expression together with MAP Kinase and Hippo pathway signalling following injury. **A**, **B**. Immunolabelling of distal sciatic nerve in control (NF2+/+) and Merlin null (NF2-/-) sciatic nerve 7d after nerve crush injury with cJun antibody (n=3 mice). Scale bar 25μm. **C**. Western blot of intact and injured distal sciatic nerves 7d after nerve cut in control and Merlin null nerves (n=3 pools, 1 pool=3 nerves from 3 mice for each genotype). Values represent normalised expression against the control for each time point. Vinculin is used as a loading control. **D**. Western blots of distal control and Merlin null nerves at 4d, 11d and 21d after nerve crush injury (n=3 pools, 1 pool=3 nerves from 3 mice for

each genotype). Values represent normalised expression against the control for each time point. Vinculin is used a loading control.

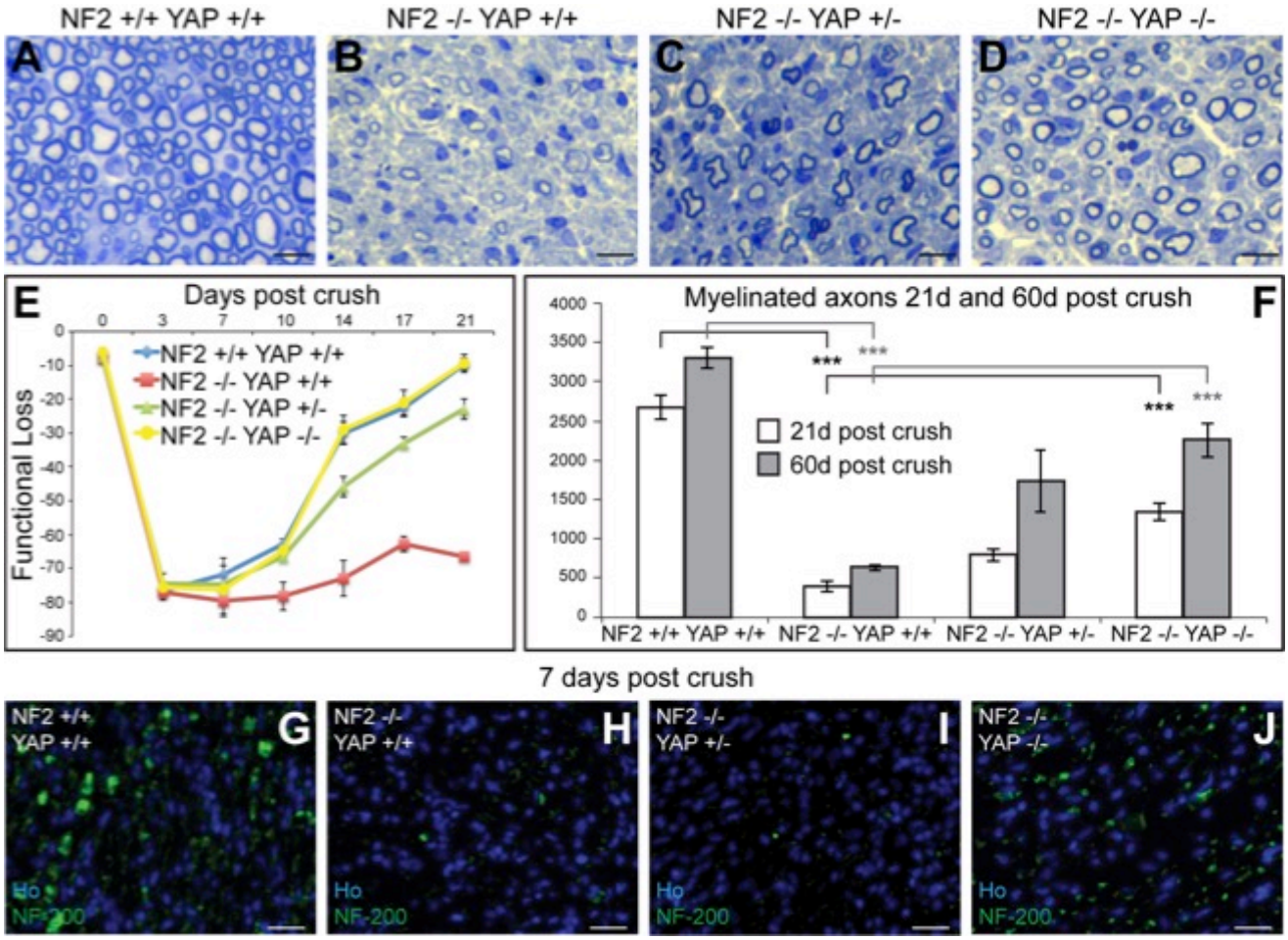

Figure 7: Loss of YAP in Merlin null Schwann cells improves both axonal repair and functional recovery following injury. **A-D**. Toluidine blue stained semi-thin sections of distal sciatic nerve at 60d post crush injury showing increased numbers of myelinated axons in NF2-/- YAP-/- double null nerves (D) compared to NF2-/- YAP+/+ Merlin single null animals (B). Mice with loss of one YAP allele (NF2-/- YAP+/-, C) have an intermediate phenotype (n=3 mice for all genotypes). Scale bar 10µm. **E**. SSI analysis of control, Merlin single null and Merlin/YAP double null animals (n=3 mice for each experiment and time point). **F**. Counts of myelinated axons in distal sciatic nerve of control, single Merlin null and Merlin/YAP double null animals at 21d (n=6 for each genotype and time point) and 60d (n=3 mice for each genotype and time point) following crush injury. **G-J**. Immunolabelling of distal sciatic nerve with neurofilament antibody in control, single Merlin null and Merlin/YAP

double null animals 7d post crush injury (n=3 mice). Scale bar 50μm. One-way ANOVA with Bonferroni's multiple comparison test ***$P \leq 0.001$ in the comparisons shown (E).

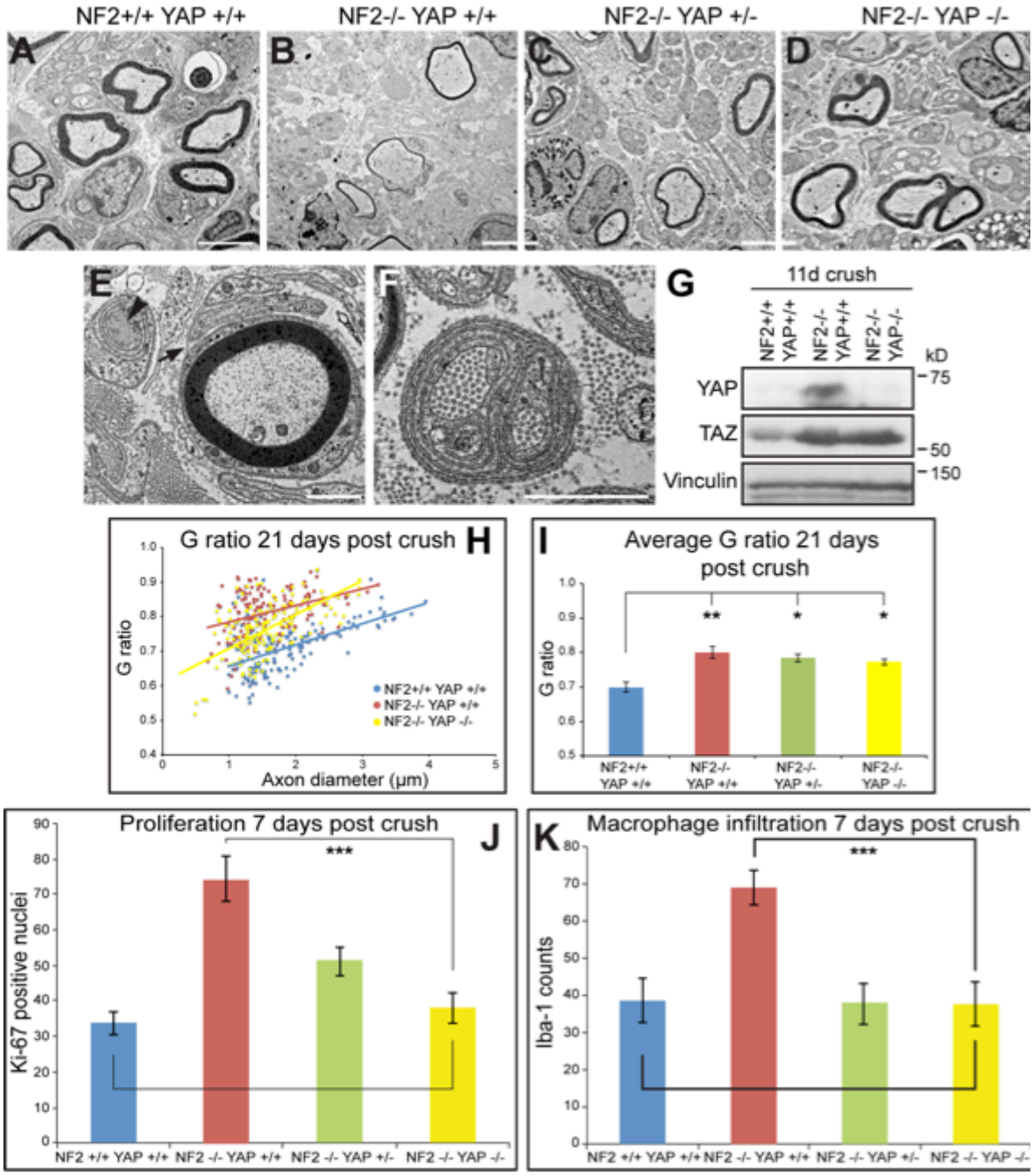

Figure 8: Morphological analysis of nerves following injury and normalisation of proliferation and macrophage infiltration in Merlin/YAP double null nerves**. A-D.** Transmission EM images of distal sciatic nerve at 21d post crush injury showing remyelination of axons in NF2-/- YAP-/- double null nerves (D) compared to NF2-/- YAP+/+ Merlin null animals (B). Mice with loss of one YAP allele (NF2-/- YAP+/-, C) have an intermediate phenotype (n=3 mice for all genotypes). Scale bar 5µm. **E, F.**

Transmission EM pictures of Merlin/YAP double null distal sciatic nerves at 21d post-injury showing Schwann cell processes and collagen wrapping by Schwann cells within the nerve. Black arrow in E showing the continuous basal lamina of a myelinating Schwann cell with Schwann cell processes inside. Black arrowhead in E points to collagen wrapping, as also observed in F (representative images from 3 biological replicates). Scale bar 1µm. **G**. Western blot 11d after nerve crush injury showing loss of YAP induction in NF2-/- YAP-/- distal sciatic nerves compared to NF2-/- YAP+/+ nerves. TAZ is upregulated in both Merlin single null and Merlin/YAP double null distal sciatic nerves compared to control nerves post injury. Vinculin is used as a loading control (n=3 pools, 1 pool=3 nerves from 3 mice for each genotype). **H, I.** Scatter plot graph (H) and average (I) G ratio measurements 21d post crush in Merlin null and Merlin/YAP double null distal sciatic nerves (n=3 mice). **J, K.** Graphs showing numbers of Ki67 positive proliferating cells (J) (n=3 mice) and numbers of Iba1 positive macrophages (K) (n=3 mice) in distal nerves of control, Merlin single null and Merlin/YAP double null animals at 7d post crush injury. One-way ANOVA with Bonferroni's multiple comparison test ***P*=0.003, **P*=0.013 compared to NF2-/- YAP+/-, **P*=0.021 compared to NF2-/- YAP-/- (F), ****P*≤0.001 in the comparisons shown (J, K), *P*=0.862 (J), *P*=0.995 (K).

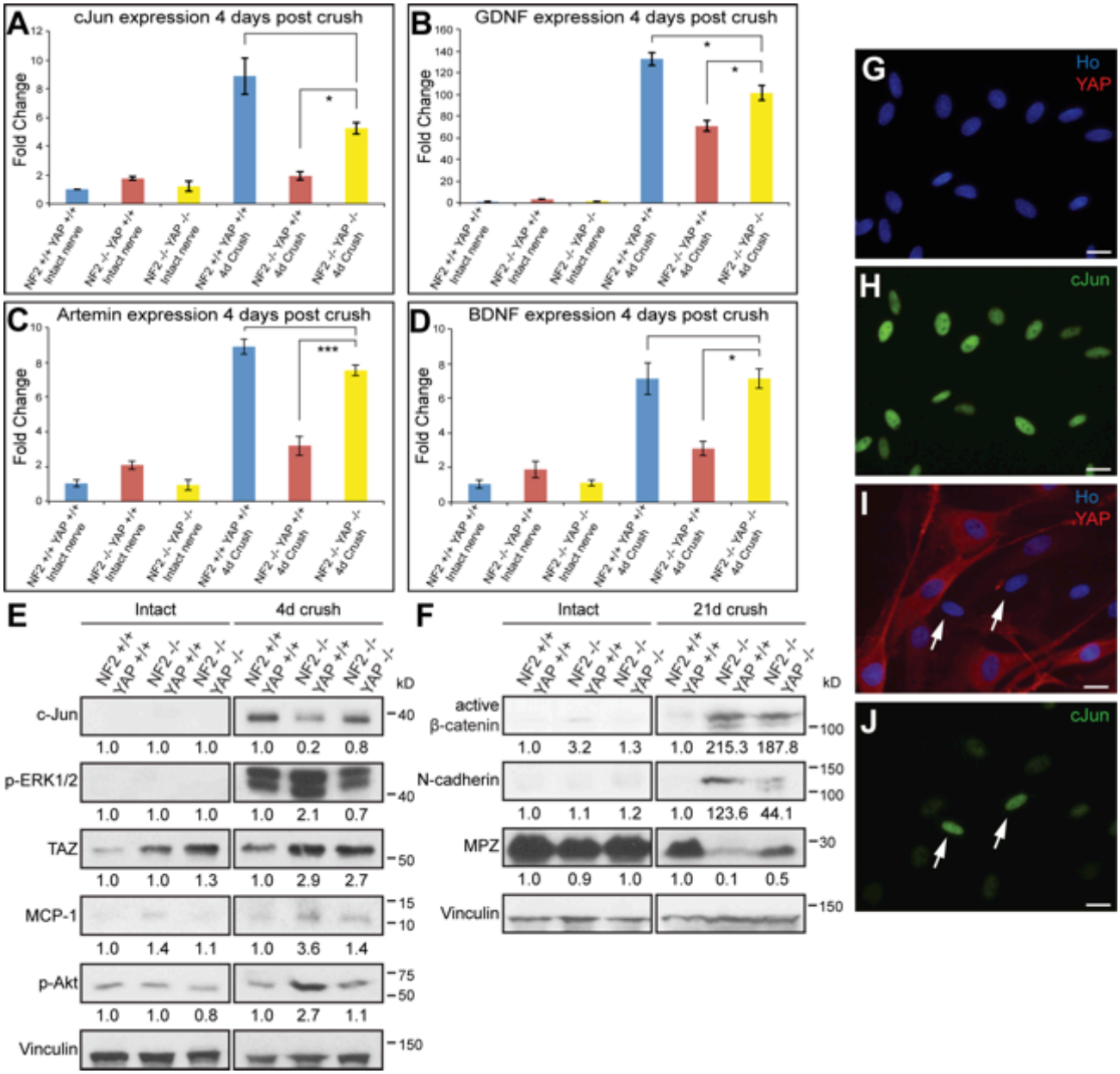

Figure 9: Loss of YAP increases both cJun and neurotrophin expression in Merlin-null Schwann cells following injury. **A-D.** Quantitative PCR measurement (n=3 pools, 1 pool=3 nerves from 3 mice for each genotype) of cJun (A) and neurotrophin (GDNF, B; Artemin, C; BDNF, D) expression 4d after crush injury in control (NF2 +/+ YAP+/+), Merlin single null (NF2-/- YAP+/+) and Merlin/YAP double null (NF2-/- YAP-/-) animals. **E**. Western blot showing cJun, p-ERK1/2, TAZ, MCP-1 and p-Akt activation in control uninjured nerves and 4d after crush injury in control, Merlin single null and Merlin/YAP double null animals (n=3 pools, 1 pool=3 nerves from 3

mice for each genotype). Values represent normalised expression against the control. Vinculin is used as a loading control. **F.** Western blot showing loss of YAP in Merlin null Schwann cells increases Myelin Protein Zero (MPZ), reduces N-cadherin expression, but does not affect levels of activated β-catenin at 21d after crush injury (n=3 pools, 1 pool=3 nerves from 3 mice for each genotype). Values represent normalised expression against the control. Vinculin is used as a loading control. **G-J**. YAP expression reduces levels of cJun in Schwann cells. Immunolabelling of rat Schwann cells expressing control LacZ (G, H) or $YAP^{Ser127Ala}$ (I, J) showing reduced levels of cJun protein in $YAP^{Ser127Ala}$ expressing cells (I, J) (n=3 experiments). Arrows in I and J indicate non-YAP-overexpressing Schwann cells with unchanged levels of cJun protein. Scale bar 20μm. One-way ANOVA with Bonferroni's multiple comparison test **P*=0.048, *P*=0.07 (A), **P*=0.033 to NF2-/- YAP+/+, **P*=0.028 to NF2+/+ YAP+/+ (B), ****P*≤0.001, *P*=0.218 (C), **P*=0.016, *P*=1 (D).

Methods

Mice.

All animal experiments conformed to UK Home Office regulations under the Animals (Scientific Procedures) Act 1986. All breeding and surgical experiments have been approved by the Plymouth University Animal Welfare and Ethical Review Board. Animals with a Schwann cell-specific null of Merlin ($NF2^{fl/fl}$-P0-CRE+) were made as previously described (Doddrell et al., 2013; Feltri et al., 1999; Giovannini et al., 2000); $NF2^{fl/fl}$-P0-CRE- littermates were used a controls. Merlin null animals were crossed with YAP conditional null ($YAP^{fl/fl}$) animals (Zhang et al., 2010) to generate Merlin null animals with loss of either one or both YAP alleles in P0-CRE+ animals; appropriate P0-CRE- animals were used as controls in these experiments. Genotyping of animals was performed as previously described (Feltri et al., 1999; Giovannini et al., 2000; Truett et al., 2000; Zhang et al., 2010). For developmental studies approximately equal numbers of male and female mice were used with the appropriate sex and age matched littermate controls.

Sciatic nerve injury, cut or crush, was carried out in adult animals, between 6 weeks and 2 months of age, under isoflurane anaesthesia as previously described (Dun and Parkinson, 2015) and distal sciatic or tibial nerve samples taken at various time points following injury; contralateral uninjured nerves were used as controls. Once more, equal numbers of male and female mice were used with the appropriate sex and age matched littermate controls for each experiment.

Electron Microscopy.

Samples for low vacuum (LV) scanning or transmission electron microscopy (SEM/TEM) were fixed in glutaraldehyde and embedded in resin blocks. For LV-SEM sample block surfaces were polished and analysed using a JEOL 6610 LV-SEM machine. For TEM, ultrathin sections were prepared, stained and visualised using a JEOL 1400 microscope. Myelin thickness or G ratio (myelin thickness/myelin + axon thickness) measurements were made from at least 200 myelinated fibres mid-sciatic nerve per animal at stated timepoints. Measurements of axon and myelinated fibre (axon + myelin) diameter were made using ImageJ software. Statistical significance difference was measured using the Mann Whitney U test.

Mouse Functional Tests.

The mouse static sciatic index (SSI) measurement (Baptista et al., 2007) was used to assess sensory-motor co-ordination in animals following sciatic nerve injury. Toe pinch tests were also used to assess recovery of sensory function (pressure sensitivity) as previously described (Arthur-Farraj et al., 2012). For single frame motion analysis to evaluate recovery of locomotor function, mice were accustomed to beam-walking 1 week prior to surgery. Here, animals walk voluntarily from one end of a horizontal beam (length 1 m; width 4 cm) towards the other end. For all mice, a rear view of one walking trial was captured with a video camera prior to surgery and at different time-points following surgery. These video sequences were examined using VirtualDub 1.6.19 software. Selected frames, in which the animals could be seen in defined phases of the step cycle, were used for measurements of the foot-base angle (FBA), as described (Fey et al., 2010).

For rotarod testing, to measure motor function, 6-8 week old animals were placed on a rotating rod which accelerated from 2 to 30 rotations per minute over a time period of 250 seconds. The time taken for the animal to fall off (latency) was measured and recorded (Kuhn et al., 1995).

Electrophysiology.

Investigation of sciatic nerve conduction characteristics was performed 5 weeks after experimental crush injury, using previously described methods (Schulz et al., 2014b). Nerve conduction velocity (NCV) tests in mice following crush injury were used to measure the efficiency of re-myelination of the in control and Merlin null mouse nerves. The compound muscle action potential (CMAP) is a measure of the number of functional axons within the repairing nerve following injury and is an indicator of an impaired axonal regeneration when significantly reduced.

In brief, mice were anesthetized using isoflurane/O_2 inhalation. Hind limb fur was removed. Constant body temperature of 37°C was maintained by a heating plate and continuously measured by a rectal thermal probe. Needle electrodes were used to stimulate the sciatic nerve at both a proximal and distal stimulation site relative to the crush site. A ring electrode recorded the neuromuscular response from the gastrocnemius muscle.

Immunocytochemistry and western blotting.

Nerve samples were fixed in 4% paraformaldehyde/PBS overnight, cryoprotected in 30% sucrose/PBS overnight at 4°C, and embedded in O.C.T. compound and frozen for cryosectioning. Sections for immunostaining (10µm) were cut using a Leica CM1860 UV cryostat. For measurement of proliferation and macrophage numbers, control and mutant nerves were mounted within the same OCT block and sections

between 3-4mm distal to the injury site, equidistant form the injury site for each genotype, were used for immunolabelling and counts. Sections were washed in PBS and blocked in either antibody diluting solution (Parkinson et al., 2004) or 10% goat serum/PBS, supplemented with 0.2% Triton X-100 before addition of primary antibody. A two or three layer labelling system was used, either directly fluorophore conjugated secondary antibody or a biotinylated secondary antibody followed by a streptavidin fluorophore conjugate. Samples were counterstained with Hoechst to reveal nuclei. Results presented for proliferation (Ki67 positive cells) and macrophage numbers (Iba1) are for the total number of positively stained cells within the nerve section. Three or more individual nerve sections of the same genotype were counted for each immunolabelling. Staining of teased nerve fibres with a fluorophore conjugated phalloidin for assessment of internodal distance and Schmidt-Lanterman incisures was performed as described previously (Sharghi-Namini et al., 2006). Wholemount staining of nerve samples after injury was performed as previously described (Dun and Parkinson, 2015). Preparation, culture and adenoviral infection of rat Schwann cells was performed as previously (Parkinson et al., 2008; Parkinson et al., 2004), using an adenovirus expressing $YAP^{Ser127Ala}$ or LacZ control (Shao et al., 2014). For western blotting, samples from control and injured nerves were frozen in liquid nitrogen. Nerves from 3 mice were grouped together for each genotype and time point to create a pooled sample. Sample extraction, gel electrophoresis and analysis were all as previously described. Equal loading of samples was ensured by both protein estimation and use of colloidal gold to stain membranes following transfer (Parkinson et al., 2004; Parkinson et al., 2003).

Primary antibodies.

The following primary antibodies were used for immunofluorescence staining at the indicated dilutions: Neurofilament (NF-200) heavy 200 kDa (1/500, Abcam ab4680), cJun (1/200, Cell Signaling Technology 9165S), Iba1 (1/300, WAKO 019-19741), F4/80 (1/300, Abcam ab16911), Ki67 (1/200, Abcam ab15580).

The following primary antibodies were used for western blotting: MPZ (1/1000, Sigma Aldrich SAB2500665), MBP (1/2000, Santa Cruz Biotechnology sc-13912), Krox20 (1/500, Covance PRB-236P-100), β-Tubulin (1/2000, Santa Cruz Biotechnology sc-134229), cJun (1/1000, Cell Signaling Technology 9165), p-cJun (1/500, Cell Signaling Technology 9261), p-Erk1/2 (1/2000, Cell Signaling Technology 9101), p-p38 (1/500, Cell Signaling Technology 4631), YAP/TAZ (1/1000, Cell Signaling Technology 8418), TAZ (1/1000, Cell Signaling Technology 4883), YAP (1/1000 Cell Signaling Technology 14074), CTGF (1/1000, Abcam ab6992), Collagen IV (1/1000, Abcam ab6586), MCP1 (1/500, Peprotech 500-P113), active β-Catenin (1/1000, Millipore 05-665), N-Cadherin (1/1000, Abcam ab76057), E-Cadherin (1/1000, BD Pharmingen Clone 36 610181), p-Akt (1/2000, Cell Signaling Technology 4060), Vinculin (1/1000, Cell Signaling Technology 4650).

Histology and Immunohistochemistry.

For hematoxylin and eosin (H&E) staining, mice were sacrificed, sciatic nerves were dissected and post-fixed in 10% formalin for 24 hr at 4°C. Sciatic nerves were cut into three segments, proximal, injury site and distal. Samples were then dehydrated in ethanol followed by xylene and embedded in paraffin. Sciatic nerve segments were cut transversally into 4 µm sections using a Leica microstat. Sciatic nerve sections were deparaffinized with xylene and rehydrated through a graded ethanol series to water before H&E (Sigma) staining. For MBP staining, the sections were

subjected to pretreatment with ethylenediamine tetraacetic acid (EDTA) pH 9.0 for 30 mins. Sections were then incubated overnight with the primary antibody goat anti-MBP (1:1000, Santa Cruz Sc-13912). Immunostaining was visualised by an avidin-biotin complex method, followed by light counterstaining with haematoxylin. For the axonal visualisation, 10 µm sections were cut and stained according to Palmgren's silver stain method. Staining with Masson's Trichrome stain was performed as per manufacturer's protocol (Abcam).

Quantitative PCR analysis.

Distal nerve stumps to the crush site were collected at day 4 post-crush injury in mice and frozen in liquid nitrogen. Nerves from three mice were grouped together for each genotype and time point to create a pooled sample. Samples were crushed and homogenised on dry ice, then lysed in QIAzol Lysis Reagent (Qiagen) and RNA was purified using miRNeasy Mini Kit (Qiagen). After RNA purification, RNA was reverse-transcribed using High Capacity RNA-to-cDNA Kit (Applied Biosystems). Quantitative PCR was then performed using the *Power* SYBR® Green PCR Master Mix (Applied Biosystems). Analysis was carried out with three technical replicates per sample. Relative expression values for each gene of interest were obtained by normalizing to Rpl13 (Pratt-Hyatt et al., 2013) and fold-changes were determined with the Livak method. Primer sequences used for qPCR have been published previously (Arthur-Farraj et al., 2012).

Statistical analysis.

Statistical analysis was performed using SPSS or Microsoft Excel. The two-sided two sample Student's *t*-test or one-way ANOVA with Bonferroni's multiple comparison test, due to the power it has for small sample sizes, were used depending on the

number of the samples. Statistical significance has been reported as * $P \leq 0.05$, ** $P \leq 0.01$, *** $P \leq 0.001$. Due to the small sample sizes (n<5 for most statistical comparisons), assumptions of how well normality and equal variances fit the data could not be reliably assessed. Sample size was not predetermined by statistical methods and randomisation was not applied. The investigators were not blinded to group allocation during the experiments because the mutant nerves display obvious behavioural and morphological characteristics following nerve injury. No samples or data were excluded from the analysis. Biological replicates were used in all the experiments and these are represented in all the data plots. The n number of each experiment has been reported in all the figures. In brief, in most cases n is defined as the number of mice from the same genotype and same experiment. Samples for western blotting and quantitative PCR were prepared by grouping nerves from three mice together for each genotype and time point to create a pooled sample. We have used pooled biological replicates for the repetition of these experiments. All data are represented in the figures as Mean values ± Standard Error of the Mean.

Online supplemental material

Fig. S1 describes the G-ratio of Merlin null nerves at an additional timepoint, post-natal day 21, and the nuclei counts in longitudinal sections of adult Merlin null nerves. Fig. S2 shows the regeneration, remyelination, collagen and tissue histology of Merlin null nerves at 8 months post injury. Fig. S3 presents the sensory recovery, as measured by toe pinch, of Merlin null animals following sciatic nerve crush injury. Fig. S4 characterises the YAP null animals prior to and post injury. Fig. S5 characterises the Merlin/YAP double null animals prior to sciatic nerve crush injury.

Supplementary data:

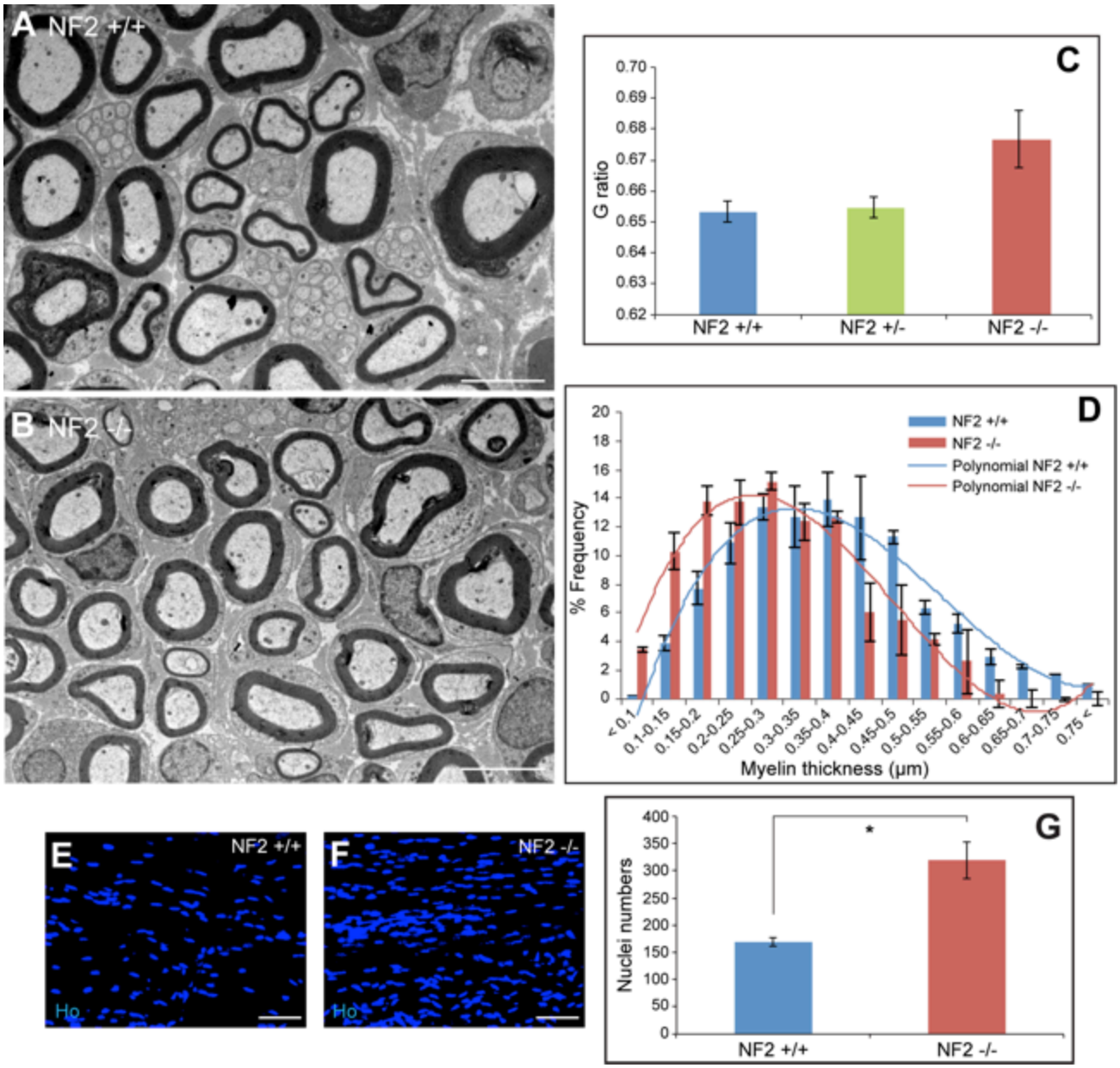

S Figure 1: Myelination and nuclei counts in nerves with Schwann cell-specific loss of Merlin. **A**, **B**. TEM pictures of P21 control (NF2+/+, A) and Merlin null (NF2-/-, B) nerves (n=3 mice). Scale bar 5µm. **C**. G-ratio measurements of sciatic nerves from P21 control, Merlin heterozygous (NF2+/-) and Merlin null nerves (n=3 mice). **D**. Graph showing distribution of myelin thickness in P6 control and Merlin null nerves (n=3 mice). **E-G**. Hoechst stained nuclei (E, F) and quantification (G) of longitudinal

cryostat sections from adult intact sciatic nerves showing increase in cell number in Merlin null (F) compared to control (E) nerves; (NF2+/+ n=3, NF2-/- n=5). Two-sided Two-Sample Student's *t* test **P*=0.017 (G).

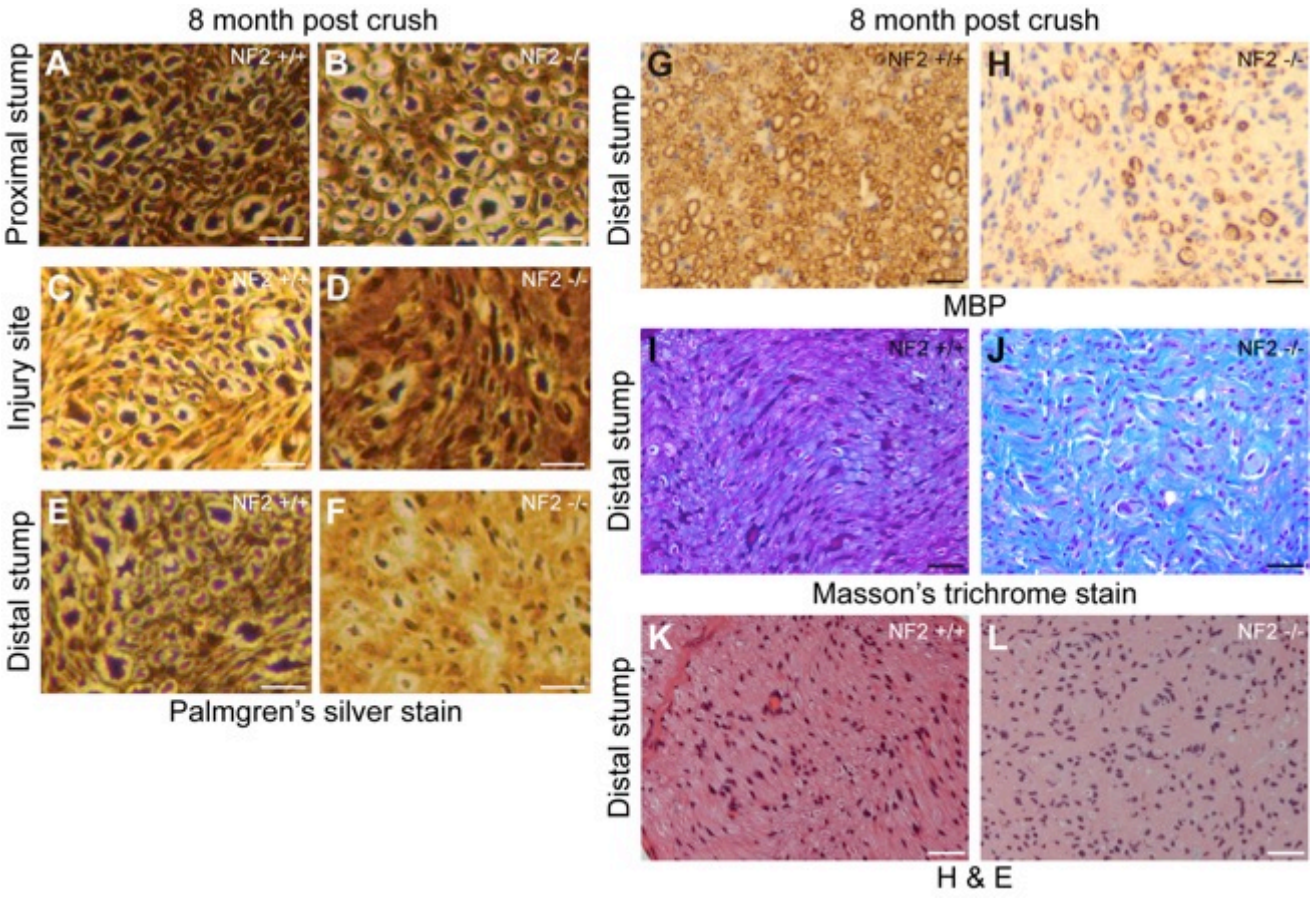

S Figure 2: Axonal regeneration, remyelination and histology of control and Merlin-null nerves eight months after injury. **A-F.** Palmgren's silver stain to show axonal regeneration in control (NF2+/+; A, C and E) and Merlin-null (NF2-/-; B, D and F) nerves at 8 months after crush injury. Sections of proximal nerve (A, B), injury site (C, D) and distal nerve (E, F) were stained to visualise axons with Palmgren's silver stain (n=6 mice). Scale bar 10μm. **G**, **H**. MBP immunolabelling of sections of control (G) and Merlin null (H) distal sciatic nerve showing low levels of MBP-positive remyelinated fibres in Merlin null nerves at 8 months post-injury (n=6 mice). Scale bar 50μm. **I, J.** Masson's trichrome stain to show collagen deposition (blue) in control (I) and Merlin null (J) distal nerves at 8 months post-injury. Masson's trichrome stains the connective tissue blue and the cytoplasm red. Scale bar 50μm. **K**, **L**.

Haematoxylin and eosin (H & E) stain of control (K) and Merlin null (L) distal nerves at 8 months post-injury (n=6 mice). Scale bar 50μm.

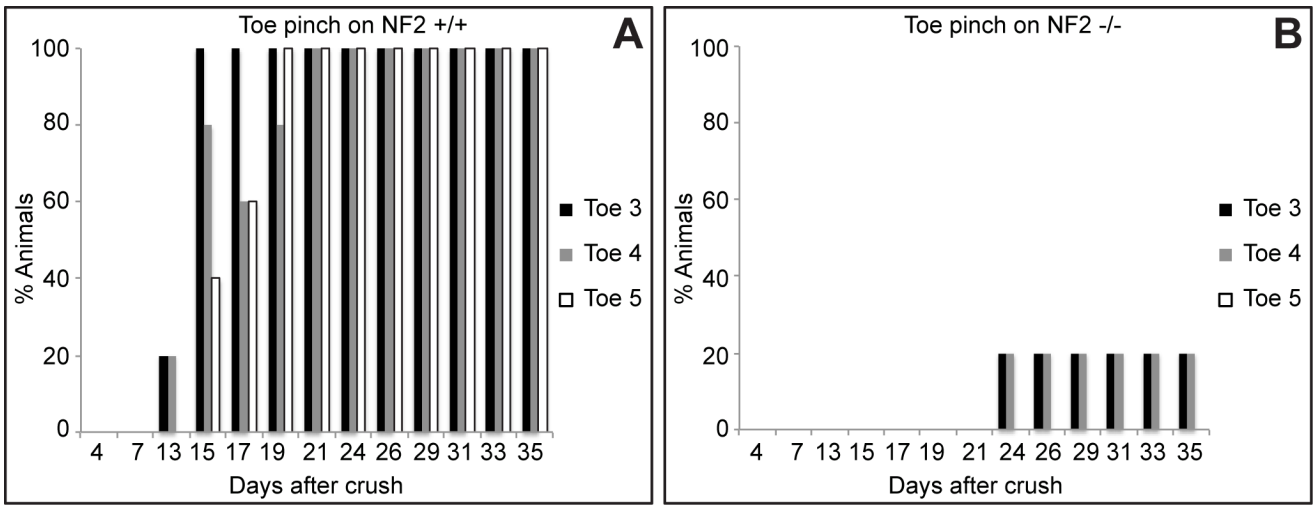

S Figure 3: Functional sensory testing of control and Merlin null animals following crush injury. **A**, **B**. Graph of toe pinch data to measure sensory recovery at timepoints up to 35d following injury for control (NF2+/+, A) and Merlin null (NF2-/-, B) animals (n=5 mice).

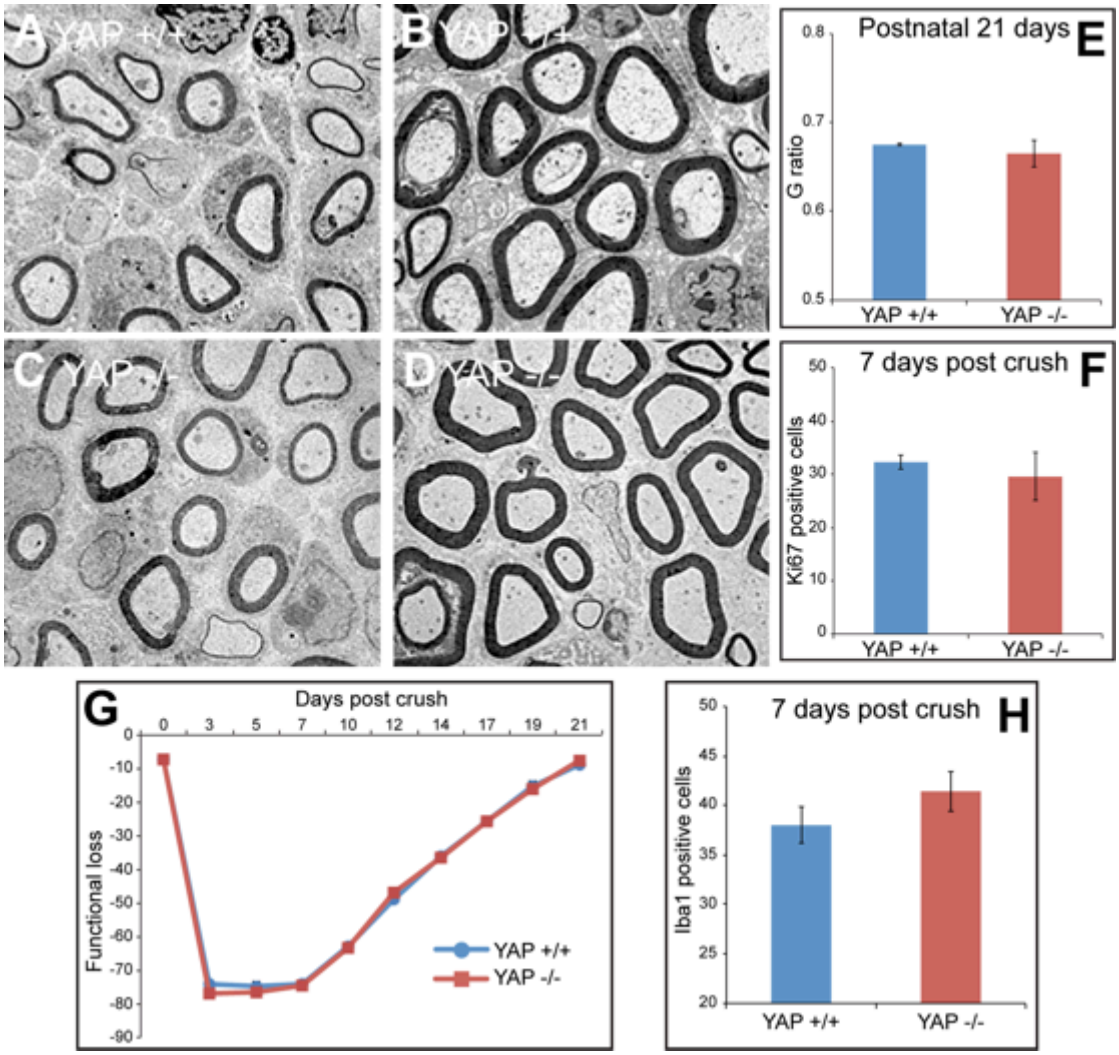

S Figure 4: Characterisation of YAP single null animals prior to and post injury. **A-D**. Transmission EM pictures of P6 (A, C) and P21 (B, D) sciatic nerves from control (YAP+/+, A, B) and YAP null (YAP-/-, C, D) animals (n=3 mice). **E**. G ratio measurements of control and YAP null animals at P21 (n=4 mice). **F**. Counts of cell proliferation in distal nerve 7d after nerve crush injury (n=3 mice). **G.** SSI measurements of control and YAP null animals up to 21d following nerve crush injury (n=3 mice). **H**. Numbers of Iba1 positive macrophages in the distal nerve at 7d after nerve crush injury in control and YAP null animals (n=3 mice). Two-sided Two-Sample Student's *t* test *P*=0.525 (E), *P*=0.27 (F), *P*=0.252 (H).

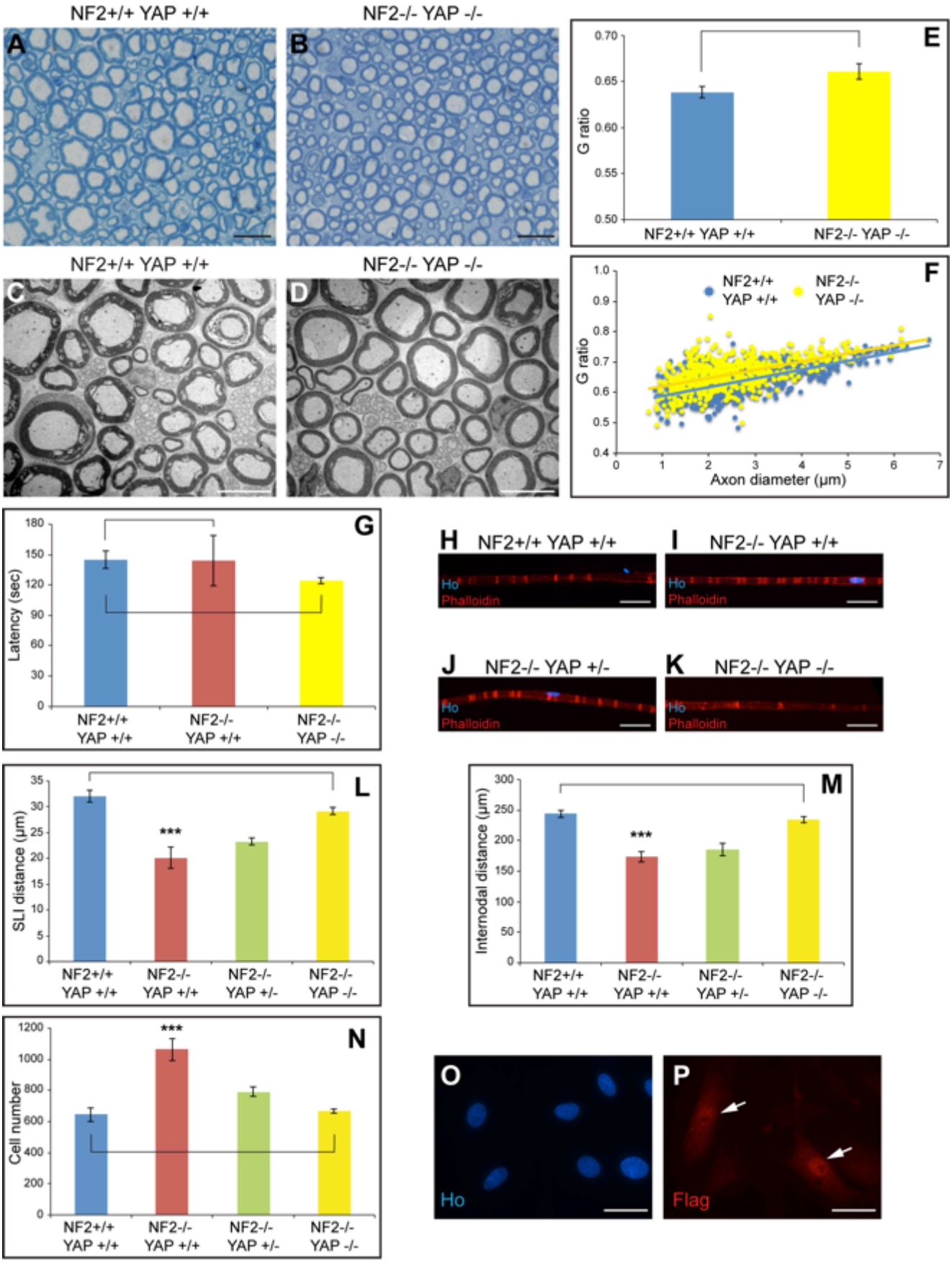
NF2+/+ YAP +/+
NF2-/- YAP -/-
A
B
C
D
E
F
G
H
I
J
K
L
M
N
O
P
G ratio
Axon diameter (µm)
Latency (sec)
SLI distance (µm)
Internodal distance (µm)
Cell number
NF2+/+ YAP +/+
NF2-/- YAP +/+
NF2-/- YAP +/-
NF2-/- YAP -/-
Ho
Phalloidin
Flag
***

S Figure 5: Characterisation of adult Merlin/YAP double null sciatic nerves. **A, B**. Toluidine blue stained semi-thin sections of adult control (NF2+/+ YAP+/+, A) and Merlin/YAP double null (NF2-/- YAP-/-, B) sciatic nerves. Scale bar 10μm. **C, D**. Transmission EM images of adult control (C) and Merlin/YAP double null (D) sciatic nerves. Scale bar 5μm. **E, F**. G ratio measurements of control and Merlin/YAP null nerves showing average (E) and scatter plot of axon diameter vs G ratio (F) (n=3 mice per genotype). **G**. Results of the rotarod test showing latency to fall on adult control, Merlin single null and Merlin/YAP double null animals. **H-K**. Phalloidin staining of teased nerve fibres of sciatic nerve visualising Schmidt-Lanterman incisures in control, Merlin single null and Merlin/YAP double null adult nerves. Scale bar 25μm. **L-N.** Loss of YAP in Merlin null nerves normalises the distance between adjacent Schmidt-Lanterman incisures (L), internodal distance (M) in teased nerve fibres and cell number (counts of Hoechst stained nuclei in transverse cryostat sections (N)) at P60 (n=4 mice). **O, P**. Hoechst (O) and Flag (P) immunolabelling of rat Schwann cells expressing $YAP^{Ser127Ala}$ (n=3 experiments). Arrows in P indicate Flag-labelled YAP-overexpressing rat Schwann cells showing clear cytoplasmic and nuclear localisation of the $YAP^{Ser127Ala}$ protein. Scale bar 10μm. Two-sided Two-Sample Student's *t* test *P*=0.103 (E). One-way ANOVA with Bonferroni's multiple comparison test *P*=1 for NF2-/- YAP+/+ and *P*=0.659 for NF2-/- YAP-/- compared to NF2+/+ YAP+/+ (E), ***$P \leq 0.001$ (L-N) for NF2-/- YAP+/+ compared to the other genotypes. *P*=0.626 (L), *P*=1 (M, N) for NF2-/- YAP-/- compared to NF2+/+ YAP+/+.